

Suspended sediment transport along the Dutch coast near IJmuiden

Evert Wielsma
Student 0424153

Faculty of Geosciences
University Utrecht

Supervisors: Dr. M. Van der Vegt (UU)
Dr. J. Nauw (NIOZ)

December 2009



Universiteit Utrecht



**Royal Netherlands institute for Sea
Research**

Abstract

The Rotterdam harbour is to be extended into the North Sea. This changes the outflow of the river Rhine into the North Sea. Measurements with an ADCP were done during 5 months at 1 location in front of the Dutch coast near IJmuiden to investigate whether changes in outflow of the river Rhine could also change suspended sediment transport along the Dutch coast and into the Wadden Sea, which is the main goal of this thesis. Measurements of the hydrodynamics and suspended sediment concentration along the Dutch coast are used to determine the processes involved in suspended sediment transport along the Dutch coast. A conclusion on the effect of the change of the outflow of the Rhine can be given when these processes are known.

There is a cross-shore circulation cell in front of the Dutch coast, when turbulence in the water column is small. This could be related to the fresh water input of the river Rhine and a resulting stratification of the water column. With large turbulence, the water column will be mixed and no stratification will be developed. Remarkable is one period when turbulence is large and the cross-shore circulation is observed. This could be related to a large input of fresh water into the North Sea.

Suspended sediment transport direction is determined by the residual current direction, which is to a large extent determined by wind direction. The periods with large cross-shore circulation do not contribute to the transport of suspended sediment as turbulence is low during these periods and with low turbulence the concentration will also be low.

This concludes that fresh water input by the river Rhine does influence the hydrodynamics along the Dutch coast, but it hardly influences the suspended sediment transport. A change in outflow of the river Rhine into the North Sea does not change the suspended sediment transport along the Dutch coast.

Acknowledgements

First of all, I would like to extend my sincere gratitude to both of my supervisors: Dr. Maarten van der Vegt and Dr. Janine Nauw. They both helped to structure the large amount of data and get the best results out of it. I would also like to thank them for guiding me through the writing of the thesis.

I would like to thank the NIOZ for providing a very comfortable working place and housing on Texel. Also many thanks to all my colleagues at the NIOZ for the nice conversations during the lunches and coffee breaks.

Finally I would like to thank my close friends and family for their support and motivation, but most of all, their interest in this research. This helped me very much accomplishing the final result.

To all these folks, I offer heartfelt thanks!

Table of contents

LIST OF FIGURES	6
LIST OF TABLES	8
1. INTRODUCTION	9
1.1 The River Rhine	9
1.2 The Rhine plume	9
1.3 The Dutch coast	10
1.4 The Wadden Sea	12
1.5 Research outline	12
2. INSTRUMENTATION:	14
2.1 ADCP	14
2.2 CTD	16
2.3 ALEC	17
2.4 CTD/OBS calibration measurement	17
3. METHODS	18
3.1 Waterlevel calculation	18
3.2 Calibration of ADCP for suspended sediment concentration	19
3.2.1 Classical regime	19
3.2.2 Turbulent regime	20
3.2.3 Calibration of ADCP (k_t)	22
3.2.4 Extrapolation of data	25
3.3 Indication of stratification	29
3.4 Harmonic analysis	31
4 DATA:	33
4.1 Meteorological data	33
4.2 Wave data	33
4.3 Salinity data	33

4.4	River discharge -----	33
5.	HYDRODYNAMICS -----	36
5.1	Tide-----	38
5.2	Residual current -----	41
5.2.1	Wind effects on the residual current -----	42
5.2.2	Buoyancy effects on the residual current -----	44
6.	SUSPENDED SEDIMENT -----	49
6.2	Suspended sediment transport-----	52
7.	DISCUSSION -----	61
7.1	ADCP calibration -----	61
7.2	Hydrodynamics-----	63
7.3	Suspended sediment -----	64
7.4	Influence of Rhine outflow on suspended sediment transport-----	65
8.	CONCLUSIONS -----	66
8.1	Hydrodynamics-----	66
8.2	Suspended Sediment -----	66
9.	LITERATURE -----	68
9.2	Literature-----	68
9.2	Websites-----	70

List of figures

figure	Title	page
Figure 1.1:	<i>The Netherlands with the Rhine entering the Dutch border near Lobith and the Nieuwe Waterweg and the Haringvliet at the downstream part of the Rhine. Also indicated are the measurement locations and the inlet at the Wadden Sea: the Marsdiep.</i>	10
Figure 1.2:	<i>(a) Salinity gradients during a survey near Noordwijk with lines of equal salinity and (b) the resulting density driven circulation (after Joordens et al., 2001)).</i>	11
Figure 2.1:	<i>Bottom mounted ADCP after a few months in sea</i>	14
Figure 2.2:	<i>Backscattered sound, two Doppler shifts, (A) one from the transducer to the particles (scatters), and (B) a second on the way back after reflection (Gordon, 1996).</i>	15
Figure 2.3:	<i>Schematic side view of the bottom mounted ADCP</i>	15
Figure 3.1:	<i>Water level during the first month of the deployment at the measurement location measured by the ADCP and the CTD.</i>	18
Figure 3.2:	<i>A schematic representation of backscattering from particles (indicated by dots) that are (a) randomly distributed and (b) that have a patchiness on length scales comparable to the incoming acoustic waves. The direction of the incoming sound waves is downward in this figure (Merckelbach and Ridderinkhof, 2006)</i>	20
Figure 3.3:	<i>A schematic picture of a turbulent eddy generating a concentration fluctuation from a concentration gradient (Merckelbach and Ridderinkhof, 2006).</i>	20
Figure 3.4:	<i>The correlation between the suspended sediment concentration of the water samples and the measured Volt by the OBS. The dots represent the measurements and the black line is the linear correlation.</i>	23
Figure 3.5:	<i>(A) Suspended sediment concentration in mg/L measured by the OBS and (B) Suspended sediment concentration in mg/L measured by the ADCP</i>	26
Figure 3.6:	<i>Linear regression between total suspended sediment derived from the ADCP and the suspended sediment concentration measured with the OBS during the calibration measurement.</i>	27
Figure 3.7:	<i>Absolute depth averaged velocities during the calibration measurement</i>	27
Figure 3.8:	<i>Concentration (mg/L) from ALEC in the top figure and concentration (mg/L) from the second lowest bin of the ADCP in the lower figure for $\gamma = 0.8$.</i>	28
Figure 3.9:	<i>Mean concentration profile with the solid line representing the measured concentration and the dashed line the extrapolated concentration.</i>	28
Figure 3.10:	<i>Bottom boundary layer with a) idealized situation and B) stratified situation, with shear plane at bottom boundary layer (Simpson and Souza, 1995).</i>	31
Figure 4.1:	<i>Wind direction and relative duration of the direction during ADCP deployment. Colours indicate the wind speed classes.</i>	34
Figure 4.2:	<i>Wave direction and relative duration of the direction during ADCP deployment. Colours indicate the wave height classes.</i>	34

Figure 4.3:	Salinity (psu) at 1.5 m above the seabed near the ADCP in 2007 (top) and river discharge at Lobith in m ³ /s in 2007.	35
Figure 5.1:	Cross-shore (left) and alongshore (right) time averaged current over the whole measurement period, 288 M2 tidal cycles, where velocities to the east (onshore) and north (alongshore) are positive and velocities to the west (offshore) and south (alongshore) are negative.	37
Figure 5.2:	The correlation (r^2) between the measured velocities and the predicted tide with the M1, M2, M4, M6 and M8 tidal constituent.	38
Figure 5.3:	Measured (a) alongshore and (b) cross-shore velocities over depth during 2 M2 tidal cycles on day 237.	40
Figure 5.4:	The tidal prediction on day 237 from the M1, M2, M4 M6 and M8 constituent. Positive values indicate flood, negative values indicate ebb.	40
Figure 5.5:	The residual depth averaged current over 25 hours, two M2 tidal cycles, during the whole measurement period for the alongshore current (top figure) and the cross-shore current (bottom figure).	41
Figure 5.6:	The difference between top and bottom velocity in the cross-shore direction, averaged at each time step over two M2 tidal cycles during the whole measurement period.	42
Figure 5.7:	Residual depth averaged velocities, with a) averaged over total measurement period and b-e) averaged over periods with dominant wind direction.	43
Figure 5.8:	Tidal ellipses near the bottom and near the surface for 1 M2 tidal cycle on day 323. The red arrow indicates the direction of the tidal ellipse.	46
Figure 5.9:	Ellipticity during the measurement period with negative values indicating clockwise motion and positive values anticlockwise motion.	46
Figure 5.10:	a) Ellipticity difference between bottom (2 meter above the seabed) and top (2 meter from the surface) (-), b) Absolute difference in residual cross-shore velocity between top and bottom (m/s), c) Alongshore M2 and S2 current amplitudes (m/s), d) Wave height (m), e) wind velocity (m/s) and f) River discharge near Lobith (m ³ /s). Vertical lines indicate peaks in ellipticity.	47
Figure 5.11:	Correlation between the ellipticity difference in the top and bottom of the water column and the velocity difference in the cross-shore direction in the top and bottom of the water column. Both velocity difference and ellipticity are averaged over two M2 tidal cycles. The r^2 is 0.68.	48
Figure 5.12:	Velocities in cross-shore direction with positive values directed onshore (top), predicted velocities with the M1, M2, M4, M6 and M8 tidal constituent (middle) and ellipticity (bottom). The results are shown for a 4 day period with changing tidal ellipse properties.	48
Figure 6.1:	Depth averaged suspended sediment concentration during the whole measurement period.	49
Figure 6.2:	Measured suspended sediment concentration (top), predicted suspended sediment concentration with the M1, M2, M4, M6 and M8 tidal constituent (middle) and the mean suspended sediment concentration, calculated with a walking average over 2M2 tidal cycles (bottom). These plots were made from day 320 to 325.	50
Figure 6.3:	Correlation between measured depth averaged suspended sediment concentrations and predicted depth averaged suspended sediment concentration	50
Figure 6.4:	The wave height averaged over each 25 hours and the suspended sediment concentration averaged over each 25 hours. The red line indicates the linear	51

correlation between the two parameters.

Figure 6.5:	(a) Measured suspended sediment transport in the alongshore (positive to the north) during the whole measurement period, (b) predicted suspended sediment transport according to equation 6.2, (c) difference between measured and predicted transport, (d) the mean suspended sediment transport, (d&e) the suspended sediment transport by the M2 and M4 tidal cycle. All in $\text{kg}/(\text{m}^2\text{s})$.	56
Figure 6.6:	(a) Measured suspended sediment transport in the cross-shore (positive onshore) during the whole measurement period, (b) predicted suspended sediment transport according to equation 6.2, (c) difference between measured and predicted transport, (d) the mean suspended sediment transport, (d&e) the suspended sediment transport by the M2 and M4 tidal cycle. Note: The scale is ten times as small as in figure 6.5, the alongshore suspended sediment transport. All in $\text{kg}/(\text{m}^2\text{s})$.	57
Figure 6.7:	Suspended sediment transport in the alongshore and cross-shore (top) plotted together with the wind direction in degrees from the north, wind speed in m/s and wave height in m, for 14 days.	58
Figure 6.8:	(A and B) The absolute dominance the transport by tidal asymmetry versus the residual transport of the suspended, value of 1 indicating a dominance of residual transport, value of -1 indicating dominance by tidal asymmetry. (C and D) Same as A and B, but than relative dominance, with a value of 1 indicating both residual as tidal asymmetry flux to the north, a value of -1 indicating both residual as tidal asymmetry flux to the south and a value of 0 indicating opposing directions.	59
Figure 6.9:	(A) Velocity in the cross-shore, (B) suspended sediment concentration and (C) wave height during 5 days with and without high cross-shore velocity differences.	60
Figure 7.1:	Alongshore velocities, depth averaged suspended sediment concentration and depth averaged suspended sediment transport with $\gamma=0.4$, $\gamma=0.8$ and $\gamma=1.0$ for two M2 tidal cycles. The green line is on top of the red line, the red line is on top of the blue line.	61

List of tables

Table	Title	page
Table 2.1:	list of instruments and the measured parameters of the instruments	16
Table 3.1:	Basic tidal periods of astronomical motions (Puch, 1987)	32
Table 3.2:	Main tidal constituents (Puch, 1987)	32
Table 3.3:	Shallow water constituents (Puch, 1987)	32
Table 5.1:	Measured velocities in which positive values indicate an alongshore current to the north and a cross-shore current to the east (towards the coast).	36
Table 5.2:	Main tidal constituents of the depth averaged alongshore velocities over the whole measurement period ($r^2=0.90$)	39
Table 5.3:	Main tidal constituents of the depth averaged cross-shore velocities over the whole measurement period ($r^2=0.24$)	39

1. Introduction

The Rotterdam harbour is to be extended in the offshore direction. The first plans for this extension were rejected as it could not be proven that the extension will not have any effect on the transport of suspended sediment and larvae along the Dutch coast to the Wadden Sea. The Wadden Sea is a protected area by European law. The extension of the harbour will change the outflow of fresh water from the river Rhine into the Dutch coastal zone. As the input of fresh water into the North Sea influences current patterns, a change in this input could also change the transport of suspended sediment along the Dutch coast and thus change the import of suspended sediment into the Wadden Sea.

The goal of this thesis is to investigate the suspended sediment transport along the Dutch coast and to investigate whether a different input of buoyant Rhine water can result in a different input of suspended sediment into the Wadden Sea. First the processes and measurements done in the area will be discussed. This will lead to the research questions of this thesis.

1.1 The River Rhine

The Rhine enters the Netherlands near Lobith. The average Rhine discharge is 2200 m³/s. The discharge can be up to 12.000 m³/s during winter, measured in 1995, and as low as 1000 m³/s during summer (Middelkoop, 1998). It takes two days before water passing Lobith reaches the North Sea basin (Terwindt, 1967). The average suspended sediment load near Lobith is 30 mg/L (Asselman, 1998). The suspended sediment concentration is 10-20 mg/L at the downstream part of the Rhine, in the Nieuwe Waterweg and the Haringvliet (Rijkswaterstaat; figure 1.1).

1.2 The Rhine plume

A buoyant plume of the Rhine develops on top of the denser water of the North Sea. Buoyancy is the force that keeps the fresh water floating. The part of the shelf sea adjacent to an estuary where freshwater from river run-off contributes an important input of buoyancy is called the region of freshwater influence, the ROFI. The important input of buoyancy means that there needs to be enough fresh water to keep it floating on more saline water. A ROFI exists when river water, like the Rhine, enters a saline basin, like the North Sea. In this region the current patterns are governed by density differences between salt sea water and fresh river water (Simpson, 1997).

There are different estimates of the dimensions of the Rhine plume. According to Van Alphen (1988) the Rhine plume is 4 to 10 meters deep and 5-10 km wide and can reach

up to 40 km north of the outflow point. According to De Boer et al. (in press) the Rhine plume is up to 30 km wide and can reach up to 100 km north of the outflow, reaching Texel and the Marsdiep inlet (figure 1.1). These differences in estimates occur due to different measurement of indications of the plume. Van Alphen (1988) uses salinity measurements, while De Boer et al. (in press) use water temperature measurements. The plume dimensions are also different over time and both researches use measurements on a limited time scale.

Stratified periods due to the input of buoyant water are visible near Noordwijk. There is stratification during flood and no stratification during ebb (Joordens et al, 2001). During spring tide, when current amplitudes are high, there is high tidal stirring with reversing tide. This limits the development of stratification (Simpson, 1997). Maximum stratification occurs a few days after neap, when there is a lot of fresh water in the North Sea which is not mixed yet (Simpson, 1997). Current amplitudes increase after neap and the water column will be mixed again.



Figure 1.1: The Netherlands with the Rhine entering the Dutch border near Lobith and the Nieuwe Waterweg and the Haringvliet at the downstream part of the Rhine. Also indicated are the measurement locations and the inlet of the Wadden Sea: the Marsdiep.

1.3 The Dutch coast

The residual flow in front of the Dutch coast is estimated at 10-15 m/s by Simpson (1997) and at 7-11 cm/s by Van der Giessen et al. (1990). This means that river water

that enters the North Sea reaches Noordwijk in 3 to 6 days and IJmuiden in 5.5 to 11.5 days.

The current direction and magnitude along the Dutch coast is determined by the tide, wind stresses and a buoyancy driven circulation (Van der Giessen et al., 1990). Wind will not only influence the current direction, but also result in the generation of waves and turbulence, which results in mixing of the water column (Fisher et al., 2002). During periods when mixing of the water column is large, there will be no stratification of the water column.

There is an input of suspended sediment through the Strait of Dover of 8.5 million ton/year. The input of the Flemish Banks is around 2.4 million tons/year (Van Alphen, 1990). With an average discharge of 2200 m³/s of the Rhine and an average sediment load of 30 mg/L, an average transport of 2.1 million ton per year is expected from the Rhine. However, not all the material entering the Netherlands at the Dutch-German border reaches the North Sea Basin. Most sediment settles in the downstream part of the Rhine. Measured values of import of suspended sediment to the North Sea are in the order of 0.8 million ton/year (Van Alphen, 1990). Therefore the Rhine is not an important source of suspended sediment along the Dutch coast.

The average suspended sediment concentration near the surface 1 km offshore of IJmuiden is 20 mg/L and can reach up to 45 mg/L (Visser et al., 1991). Measured suspended sediment concentrations near the surface at 10 km offshore are about 10 mg/L and decreases to 3-4 mg/L at 30 km offshore (Visser et al., 1991).

The high concentrations close to the shore are partly explained by an onshore transport of fines near the bottom and an offshore transport of fines near the surface. This will lead to a depth averaged onshore transport as concentrations near the bottom are higher. The difference in transport direction in the vertical could be caused by a density driven circulation, which implies that the Rhine does have effect on sediment transport by providing fresh water to the Dutch coastal system (figure 1.2; Visser et al. 1991).

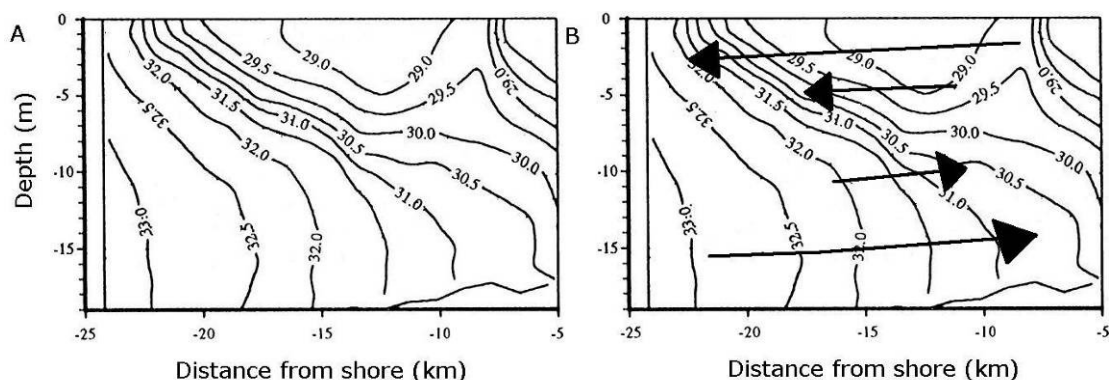


Figure 1.2: (a) Salinity gradients during a survey near Noordwijk with lines of equal salinity and (b) the resulting density driven circulation (after Joordens et al., 2001)).

1.4 The Wadden Sea

The Wadden Sea is an important sink for suspended sediment (Visser et al., 1991). Van Straaten and Kuenen (1957) concluded that there is a net import of suspended sediment into a tidal inlet due to two processes. One is the settling lag and the other is the scour lag. The time lag between the beginning of the settling of the particle and where it actually settles is called the settling lag. Scour lag is used for the phenomenon that there is a difference between the maximum velocity at which deposition of certain particles can occur and the minimum velocity at which the same material is eroded after deposition (Van Straaten and Kuenen, 1957). Both processes result in a net import of sediment into a tidal inlet.

Tidal asymmetry is also important for the import of sediment into a tidal inlet (e.g. Van de Kreeke et al., 1997, Elias et al., 2006). Due to higher velocities and resulting higher concentrations during flood, the transport is higher during flood than during ebb. So the net transport will be in the flood direction, which means import into the tidal basin.

The suspended sediment that is imported into the Wadden Sea through the Marsdiep originates from the North Sea (figure 1.1). When a different Rhine outflow can alter the suspended sediment transport along the Dutch coast, it can also alter the suspended sediment transport into the Wadden Sea.

1.5 Research outline

It is not likely that the suspended sediment input from the Rhine has a large effect on the suspended sediment transport to the North Sea. However it is possible and discussed in the literature that the buoyant water from the Rhine does have an effect on the hydrodynamics and thus also on the suspended sediment transport (e.g. Visser et al., 1991).

The suspended sediment in the Wadden Sea originates from the North Sea. Changes in suspended sediment transport along the Dutch coast result in a different import of suspended sediment into the Wadden Sea. Therefore it is of interest to measure and examine the current structure in the Rhine ROFI in combination with suspended sediment concentrations. This could give answers to the following questions which will be the main questions of this thesis:

1. Will a change in outflow of fresh water into the North Sea result in a change in suspended sediment import into the Wadden Sea?
2. What is the transport direction and magnitude of suspended sediment along the Dutch coast?

3. Which processes determine the direction and magnitude of the suspended sediment transport sediment along the Dutch coast?
4. What is the influence of the river Rhine on suspended sediment transport along the Dutch coast?

To provide an answer to these questions, measurements of both current velocities and sediment concentrations are done in the North Sea at a fixed position near IJmuiden. The measurements are taken near IJmuiden, as most measurement regarding Rhine influence were done further south, near the outflow point of the Rhine. To examine if the Rhine influences the suspended sediment transport up to Texel and the Marsdiep inlet, measurements need to be taken more close to the Texel inlet. IJmuiden is in between the outflow of the river Rhine and the Marsdiep inlet and therefore taken as the measurement location (figure 1.1).

The instruments used at this location will be discussed in chapter 2. In chapter 3 the use of the instruments and methods used in this thesis will be discussed. In chapter 4 an overview of the results of the data will be given. Chapter 5 will further discuss the hydrodynamics and chapter 6 will further discuss the suspended sediment concentration and transport. Finally, in the chapters 7 and 8 the results will be discussed and a conclusion on the suspended sediment transport along the Dutch coast near IJmuiden will be given.

2. Instrumentation:

2.1 ADCP

An Acoustic Doppler Current Profiler (ADCP) is used for this research (figure 2.1). The ADCP measures velocities in the water column by the reflection of sound waves on particles in the water column. The ADCP makes use of the Doppler Effect. The Doppler Effect is a change in the observed sound pitch that results from relative motion. An example of the Doppler Effect is the sound made by a train as it passes. The whistle has a higher pitch as the train approaches, and a lower pitch as it moves away. This change in pitch is directly proportional to how fast the train is moving. Therefore, if the pitch is measured and how much it changes, the speed of the train can be calculated (Gordon, 1996).

The ADCP sends out sound pulses. Each sound pulse will be partly reflected by particles in the water column (Merckelbach and Ridderinkhof, 2006). The frequency of the returning sound pulse will change when particles are moving (figure 2.2). The sound pulse will be Doppler shifted two times; one Doppler shift when moving towards the particles and one when the sound pulse is reflected. The ADCP measures the frequency shift and the time interval between the emitted and returning sound pulse and uses these parameters to calculate the velocity in the water column at each height.

The instrument has four transducers in different directions (figure 2.1). The beam angle between the different transducers is 30 degrees. Figure 2.3 gives a schematic view of an ADCP positioned at the bottom. The opposing transducers measure the north-south velocities and the other opposing transducers measure east-west velocities. Both sets of transducers measure the up-down velocities. The difference in up-down velocities is used as an error estimate for the velocity data.

The ADCP measures the velocity every two seconds over the whole water column. The measurements are averaged over a depth interval; a bin. The velocities of the bins are averaged over time every 15 minutes and stored in the ADCP.

The strength of the returning sound can be used to give an estimate of the amount of particles in the water and thus the suspended sediment concentration. This will further be discussed in chapter 3.



Figure 2.1: Bottom mounted ADCP after a few months in sea

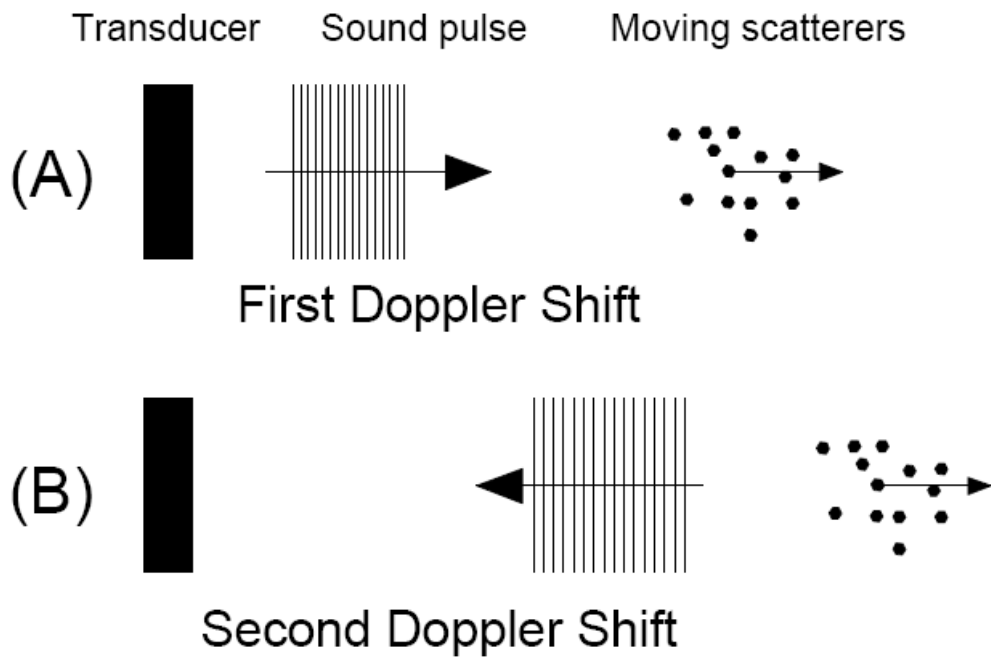


Figure 2.2: Backscattered sound, two Doppler shifts, (A) one from the transducer to the particles (scatters), and (B) a second on the way back after reflection (Gordon, 1996).

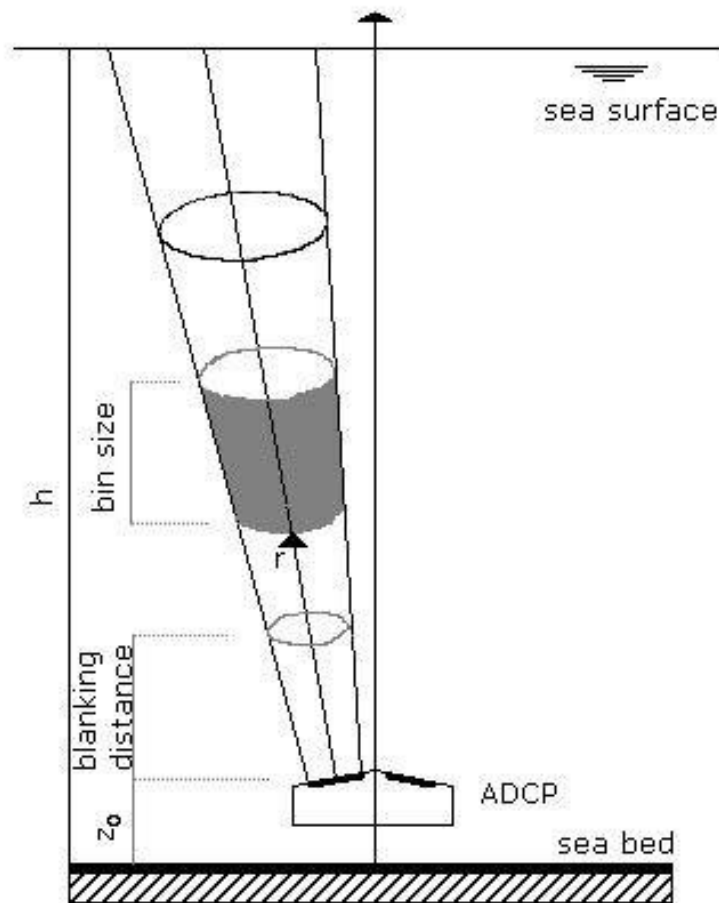


Figure 2.3: Schematic side view of the bottom mounted ADCP. The first measured bin is above the blanking distance of the ADCP.

An upward looking bottom mounted ADCP is used for this research. This means that the ADCP was positioned at the bottom of the sea, measuring the velocities from the instrument to the surface (figure 2.3). The instrument however cannot measure the velocities directly above the instrument. When the ADCP measures the velocity directly above the instrument, the sound waves would immediately return and interfere with the emitted sound pulses. By introducing a blanking distance, the ADCP has time to recover between sending out sound pulses and receiving them. This blanking distance, z_0 , is 1.28 meter. As the instrument is positioned approximately 0.25 meter above the seabed, the first bin starts at about 1.5 meter above the seabed. There are no ADCP measurements of the lowest 1.5 meter. Measurements of the lowest 1.5 meter need to be extrapolated. The bottom mounted ADCP was placed in the North Sea in front of IJmuiden. The instrument was deposited approximately 7 km offshore (figure 1.1). The measurement location is between the outflow point of the Rhine and the Wadden Sea inlet. The measurement period was between 24 August 2007 at 8:45 and 22 January 2008 at 21:00.

The ADCP was placed together with instruments which are used for a project of the NIOZ (table 2.1). The instruments include a CTD (Conductivity, Temperature and Depth) and an ALEC (turbidity meter). The ADCP was supposed to measure simultaneously with the other instrument, but due to deployment problems, the ADCP measured when the other instrument were removed, with a short overlap period.

Table 2.1: list of instruments and the measured parameters of the instruments

	ADCP	CTD	ALEC
Temperature	Temperature	Temperature	Temperature
Velocity	Velocities over water column	-	-
Suspended matter	TSM estimation from backscatter intensity over water column	-	Turbidity in ppm at 1,5 meter above the bed
Water depth	Water surface from backscatter intensity	Pressure =>depth	-
Salinity	-	Salinity at 1,5 m	-

2.2 CTD

The CTD calculates the salinity of the water by measuring the conductivity. It also measures the temperature and the density of the water. The CTD was positioned near

the ADCP at approximately 1.5 meter above the seabed. Measurements were done from February to October 2007.

2.3 ALEC

The ALEC is an OBS, Optical Backscatter Sensor, and measures the suspended sediment concentration by detecting infra-red light scattered from suspended matter. The OBS sends out an infra-red signal. This signal will scatter on particles in the water and return to the OBS. The OBS sensor measures the infra-red radiation scattered by particles in the water. With higher suspended sediment concentration, with more particles in the water, the returning signal will be stronger.

However, the returning signal is strongly dependent on the grain size. Therefore the instrument needs to be calibrated with the same sediment as near the measurement site. The signal, which is in Volt, can be transformed in a concentration in mg/L with the calibration parameters.

There is a wiper on the OBS which clears the lens before each measurement. The ALEC was positioned at approximately the same height as the CTD and measured during the same period.

2.4 CTD/OBS calibration measurement

There was a calibration measurement in November 2007 to calibrate the ADCP for suspended sediment concentrations. For this calibration an OBS and a CTD were used. The measurements with both instruments were done over the whole water column every 20 minutes. The calibration measurement lasted for 2.5 hours.

3. Methods

3.1 Waterlevel calculation

The ADCP measures a fixed range, while the water level is changing through time. This means that the ADCP also measures above the water level. Near the surface the echo intensity increases to a maximum, which is caused by air bubbles and reflection of the sound (Van Haren, 2001). The echo intensity is used to separate the data from air and sea. Separation of air and water by looking for maximum echo intensity gives an average depth of 16.89 meter. The maximum measured depth is 21 meter and the minimum is 13 meter.

The calculated depth can be compared with the measured depth of the pressure sensors from the CTD. The calculated depths from the echo intensity of the ADCP are in the range of the depth measured by the CTD and show the same pattern (figure 3.1).

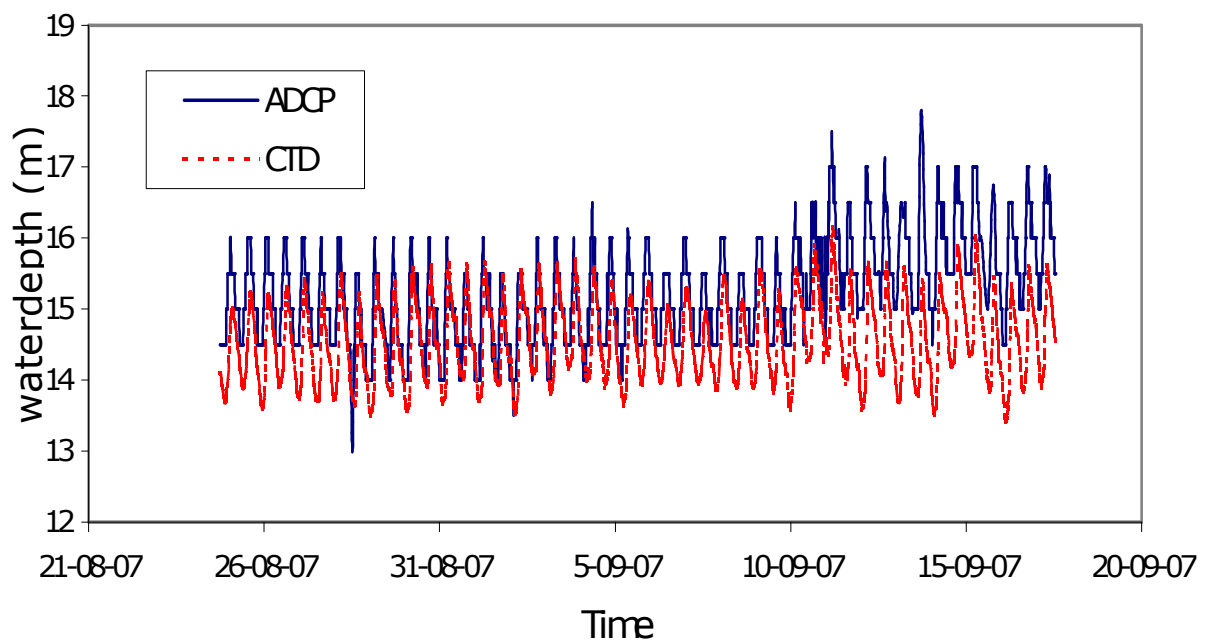


Figure 3.1: Water level measured by the ADCP and the CTD during the first weeks of the deployment at the measurement location.

3.2 Calibration of ADCP for suspended sediment concentration

3.2.1 Classical regime

Acoustic backscatter intensity is recorded by the ADCP. It is used to determine the vertical profile of the suspended sediment concentration. The pulses that reflect at particles in the water return to the ADCP (Merckelbach and Ridderinkhof, 2006). The more particles in the water, the stronger the returning signal. The strength of the signal, measured in dB, is stored in the ADCP.

The strength of the returning signal is not only affected by the amount of particles in the water, but it is also determined by acoustic wave energy losses due to geometrical spreading, attenuation by the water and the reflection efficiency by the particles. Each bin with particles has its effectiveness with respect to acoustic backscatter, which is expressed as the acoustic cross-section area per unit volume, σ (Merckelbach and Ridderinkhof, 2006):

$$\sigma = k_t * 10^{\left(\frac{k(N_c - N_t)}{10}\right)} * r^2 * e^{4r\alpha} \quad (3.1)$$

In this relation k_t is the device dependant constant which needs to be calibrated. N_c is the strength of the returning signal in counts, N_t is the threshold value, K is used to convert the strength of the returning signal from counts to dB, r^2 is correction for geometrical spreading and $e^{4r\alpha}$ is the correction for attenuation with α the attenuation factor. With this formula the acoustic cross-section per unit volume is calculated for each bin and this is used to calculate the concentrations with:

$$\sigma = \frac{25 k^4 \langle a_s^6 \rangle}{48 \pi \rho_s \langle a_s^3 \rangle} c \quad (3.2)$$

In which k is the acoustic wave number, ρ_s the density of the sediment (taken at 2650 kg/m³) and c the concentration in g/L. $\langle a_s^6 \rangle / \langle a_s^3 \rangle$ is a function of the grain size distribution where a_s is the particle size and $\langle . \rangle$ is the ensemble average over all scatters within one volume, bin (Merckelbach and Ridderinkhof, 2006).

It is assumed that all particles are randomly distributed in the water column and that the returning signal to the ADCP is also randomly distributed, which is called the classical regime (figure 3.2a). This assumption can be made when turbulence is low. Suspended particles will start to cluster in groups when turbulence gets larger, which is called the turbulent regime.

3.2.2 Turbulent regime

The phases of returning backscatter signal to the ADCP will become coherent in the turbulent regime (figure 3.2b). This is caused by turbulent eddies which change the concentration profile (figure 3.3). The suspended sediment concentration will not be evenly distributed over depth, but will increase at certain depths due to clustering of particles. The crests of sound waves of one group of the returning signal is superimposed onto crests of another group, resulting in a stronger signal picked up by the ADCP.

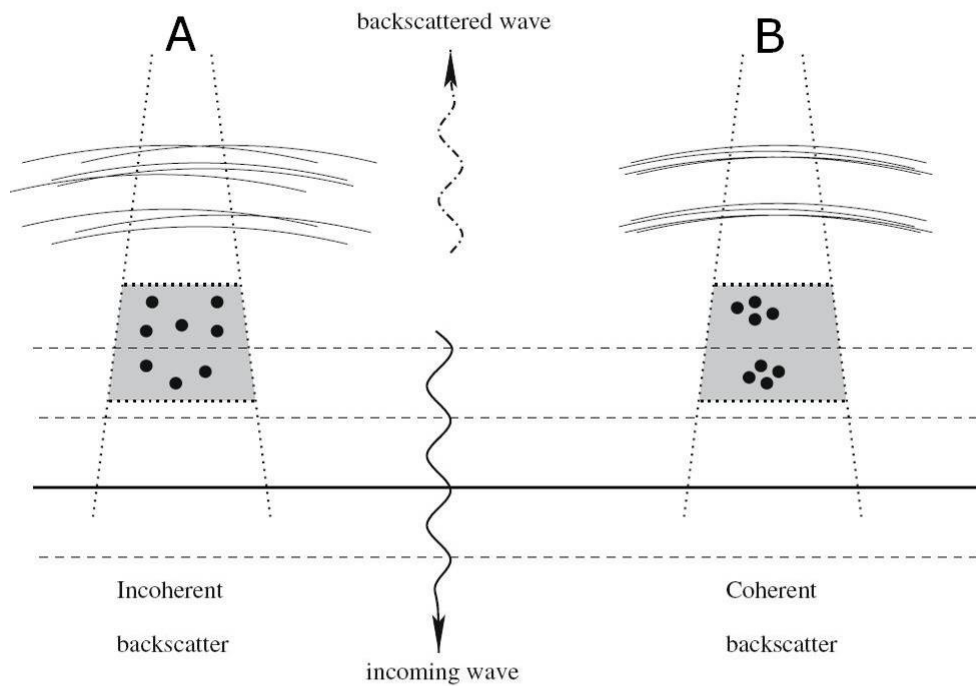


Figure 3.2: A schematic representation of backscattering from particles (indicated by dots) that are (a) randomly distributed and (b) that have a patchiness on length scales comparable to the incoming acoustic waves. The direction of the incoming sound waves is downward in this figure (Merckelbach and Ridderinkhof, 2006)

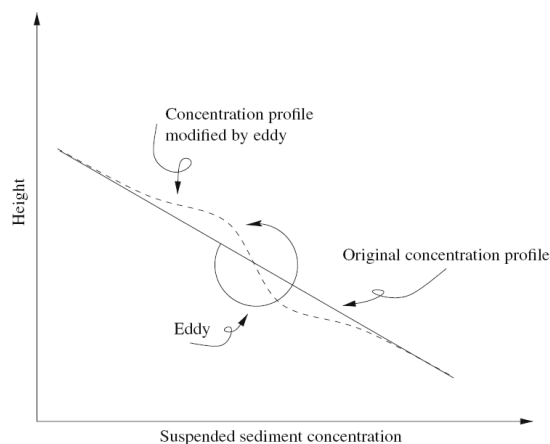


Figure 3.3: A schematic picture of a turbulent eddy generating a concentration fluctuation from a concentration gradient (Merckelbach and Ridderinkhof, 2006).

The particles start to group at the Kolmogorov length scale, the smallest scale in turbulent flow. The particles are in the turbulent regime when (Merckelbach and Ridderinkhof, 2006):

$$\gamma \lambda_k \geq \frac{2\pi}{\eta} \quad (3.3)$$

Where γ is a calibration parameter, λ_k the Bragg wave number ($=\frac{2\pi}{\lambda}$) with λ the wave length of the sound pulse of the ADCP and η is the Kolmogorov length scale. There is a calibration parameter in this equation, because this equation is site specific. This is caused by local bottom sediment characteristics. The characteristics of the sediment in the water column influences clustering of particles and therefore the transition between classic and turbulent regime is site specific.

So if the particles will be in clusters larger than the Kolmogorov length scale, particles will be in the turbulent regime. The Kolmogorov length scale is:

$$\eta = \left(\frac{\nu^2}{\varepsilon} \right)^{1/4} \quad (3.4)$$

With: ν the kinematic viscosity in $\text{m}^2 \text{s}^{-1}$ and ε the dissipation rate of turbulent energy. The dissipation rate of turbulent energy is a function of bottom roughness (bed shear velocity) and water depth (Merckelbach and Ridderinkhof, 2006):

$$\varepsilon = \frac{u_*^3}{h\kappa} \quad (3.5)$$

$$u_* \approx \frac{U}{20} \quad (3.6)$$

With u_* the bed shear velocity in m/s , h the water depth in m , κ the Von Karman constant ($=0.4$) and U the depth average velocity in m/s . So the turbulent energy is calculated with the depth average velocity and the viscosity of the water, which is taken constant.

When the sediment particles in the water are in a turbulent regime, the concentrations are not calculated with formula 3.1, but the derivative of the concentration is calculated:

$$\sigma = \frac{25}{64} \frac{k^4}{\pi^2 \rho_s^2} A \frac{\langle a_s^6 \rangle}{\langle a_s^3 \rangle \langle a_s^3 \rangle} \alpha_c \beta \left(kz \frac{h-z}{h} \right)^{2/3} K^{-5/3} \left(\frac{\partial c}{\partial z} \right)^2 \quad (3.7)$$

Where A is the surface area of the scattering volume, $\alpha_c = 0.7$, $\beta = 1$ and z = height from the bed. This formula is derived from the advection-diffusion equation by Lee (2003).

The gradients in suspended sediment concentrations in the turbulent regime can be calculated with equation 3.7. Integrating equation 3.7 gives the concentration as a function of depth apart from a constant. To determine this constant a reference concentration is calculated near the surface, where concentrations are low and the absolute error will also be relatively small. The reference concentration c is (Merckelbach and Ridderinkhof, 2006):

$$c \frac{25}{48} \frac{k^4}{\pi \rho_s} \frac{\langle a_s^6 \rangle}{\langle a_s^3 \rangle} = \left(\frac{|u_*|}{\gamma u_*} \right)^{-3.75} * \sigma \quad (3.8)$$

With σ calculated as in the traditional, non-turbulent regime. Now all concentrations during the measurement periods can be calculated. γ is site specific and can be tuned to put part of the measurement in the traditional and part in the turbulent regime (formula 3.3).

3.2.3 Calibration of ADCP (k_t)

The device dependant constant has to be calibrated to calculate the concentration from the acoustic backscatter. Therefore reference concentrations have to be measured for a certain period to calculate concentrations over the total measurement period.

A 2.5 hour calibration survey was executed on 27 November 2007. Usually a calibration survey lasts for 13 hours (one M2 tidal cycle) to measure concentrations during the whole spectrum of tidal velocities. Due to heavy weather conditions this survey had to be shortened.

CTD and OBS measurements were done every 20 minutes during this calibration measurement with the R.V. Navicula. The measurements are separated in one downcast, when the instrument goes down, and one upcast, when the instrument goes up. The downcasts are used for the calibration, as during the downcast, the water column is not disturbed yet by the instrument.

Water samples were taken more-or-less simultaneously with the OBS casts. These samples were taken to convert the measured values of Volt from the OBS to suspended

sediment in g/L (figure 3.4). This is a linear relation when concentrations are low and the suspended material is constant through time. Because the water samples were not taken directly at the same place as the OBS cast, the filtrated water samples are used to calibrate an OBS in a black box on board of the Navicula (figure 3.4). This OBS measures the suspended sediment concentration of the same water sample and is then used to calibrate the OBS mounted to the CTD.

So, first the water samples are filtrated to obtain the total amount of suspended sediment. Then the OBS in the black box is calibrated with the water samples to convert the values from Volt to g/L. This is used to calibrate the OBS, which gives values of suspended sediment over depth during the calibration cruise.

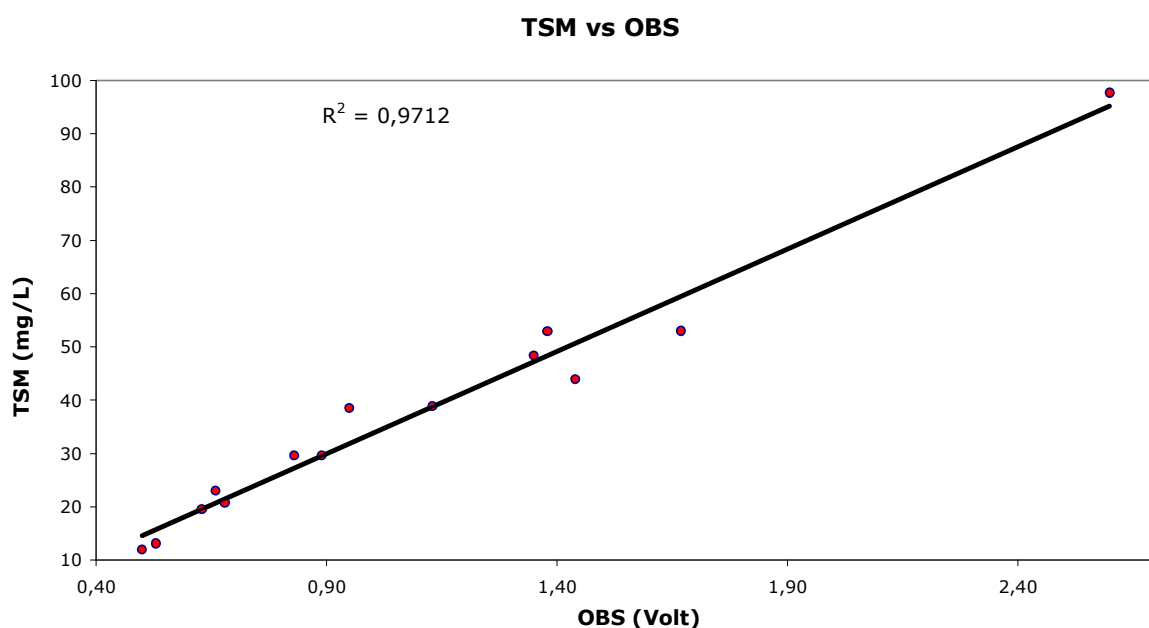


Figure 3.4: The correlation between the suspended sediment concentration of the water samples and the measured Volt by the OBS. The dots represent the measurements and the black line is the linear correlation.

The linear relation between the water samples and the OBS is in the form of $y=ax+b$, with y being the suspended sediment derived from the OBS and x the suspended sediment from the water samples. Linear regression gives values for a and b where $a_1=38.39$ and $b_1=-4,56$ (figure 3.4). Linear regression is also executed between the two OBS, with $a_2=0,74$ and $b_2=0.00$. There were rather few measurements, but the measurements were in a wide range. This made it possible to apply linear regression. After these calibrations, the suspended sediment concentration can be calculated from the OBS data (figure 3.5a).

The OBS data is linearly interpolated, to give the same bin size of 0.5 m and a 15 minute interval as the ADCP. Because the reference concentrations are known, the device dependant constant of the ADCP can be calculated. The depth average flow velocities were lower than 0.7 m/s. It is assumed that this is the lower limit for the transition to the turbulent regime in earlier studies (e.g. Merckelbach and Ridderinkhof, 2006). Therefore, the concentrations during the calibration measurement were calculated with the classical regime.

The device dependent constant k_t is calculated at $6.06 \cdot 10^{-12}$ with a standard error r^2 of 0.49 (figure 3.6). With this k_t the concentration profiles of the bottom mounted ADCP are calculated during the calibration measurement (figure 3.5b).

A part of the error can be explained by uncertainties originating from the measurements. The determination of TSM in the water samples has uncertainties of up to 7 mg/L. This is caused by errors made by filtering water samples to calibrate the OBS. But there is a larger deviation from the regression line than 7 mg/L. The overestimation by the ADCP could be caused the assumption that particles are in the classical regime, while they are in the turbulent regime.

When the calibration is executed when assuming particles are already turbulent with velocities lower than 0.6 m/s, the correlation is not improving. This is caused by the fact that around 14 h UTC time the values were most overestimated by the ADCP (figure 3.5). Tidal velocities were lowest around this period (figure 3.7).

Because the calibration measurement was executed during a period with low tidal velocities, there were no measurements done in the turbulent regime. Therefore γ could not be determined for this site with the measurements done during the calibration survey. However, the ALEC measured simultaneously with the ADCP from August to October. An estimate of γ can be made by comparing the suspended sediment concentration measured with the ALEC with the suspended sediment concentrations measured by the second lowest bin of the ADCP for different γ values. The second lowest bin of the ADCP was positioned at 2 meters above the bed, while the ALEC measured at 1.5 meter above the bed. Higher concentrations should be measured by the ALEC, as suspended sediment concentration increases towards the bottom.

Values of γ were chosen between 0.5 and 1 with steps of 0.1. The lower γ , the earlier particles get in the turbulent regime. With γ taken as 1, the concentrations measured by the ADCP are overestimated. With γ taken as 0.5 most of the suspended sediment concentrations are underestimated by the ADCP. A γ of 0.8 results in the best estimate of the total concentration during the measurement period (figure 3.8). However, this will result in a partly underestimation and overestimation of the concentration. For concentration and transport processes described further in this study a γ of 1 is taken.

With this γ the concentrations are overestimated, but the relative magnitude will be correct.

3.2.4 Extrapolation of data

The measured velocities and sediment concentrations have to be extrapolated to calculate values for velocity and suspended sediment in the lowest 1.5 meter of the water column.

The velocities decrease to zero towards the bottom. Because the lowest bin seems to give weak results, the second bin is used for the extrapolation. The velocities are linearly extrapolated from the second bin to zero at the bottom. In reality, this is probably a logarithmic, but near the bottom it will hardly differ from a straight line.

The extrapolation for the sediment concentrations is different as sediment concentrations will increase exponentially towards the bottom. Therefore, first the depth average sediment profile is discussed to try to provide a good estimate of sediment concentrations near the bottom (figure 3.9). In the lowest 4 bins, the sediment concentration seems to increase linearly, except in the lowest bin, in which the concentration decreases again. So again the lowest bin is not used for the extrapolation and the sediment concentrations are linearly extrapolated with the same gradient as between bin 4 (at 3 meter above the bed) and bin 2 (at 2 meter above the bed).

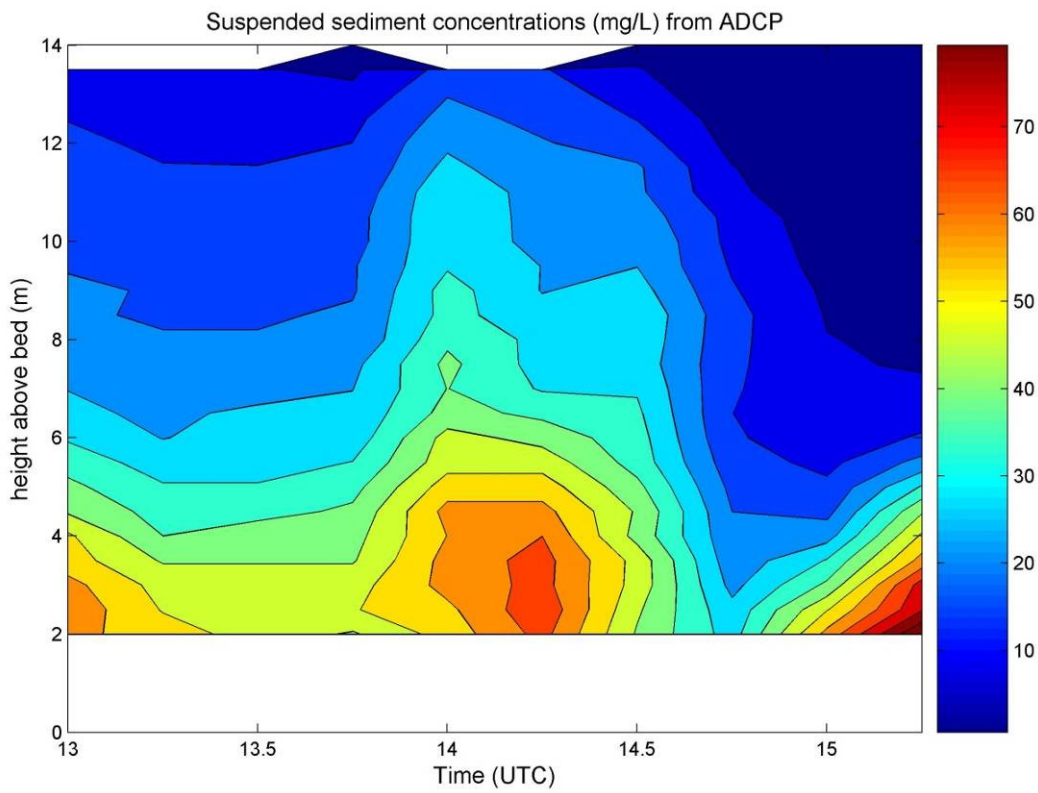
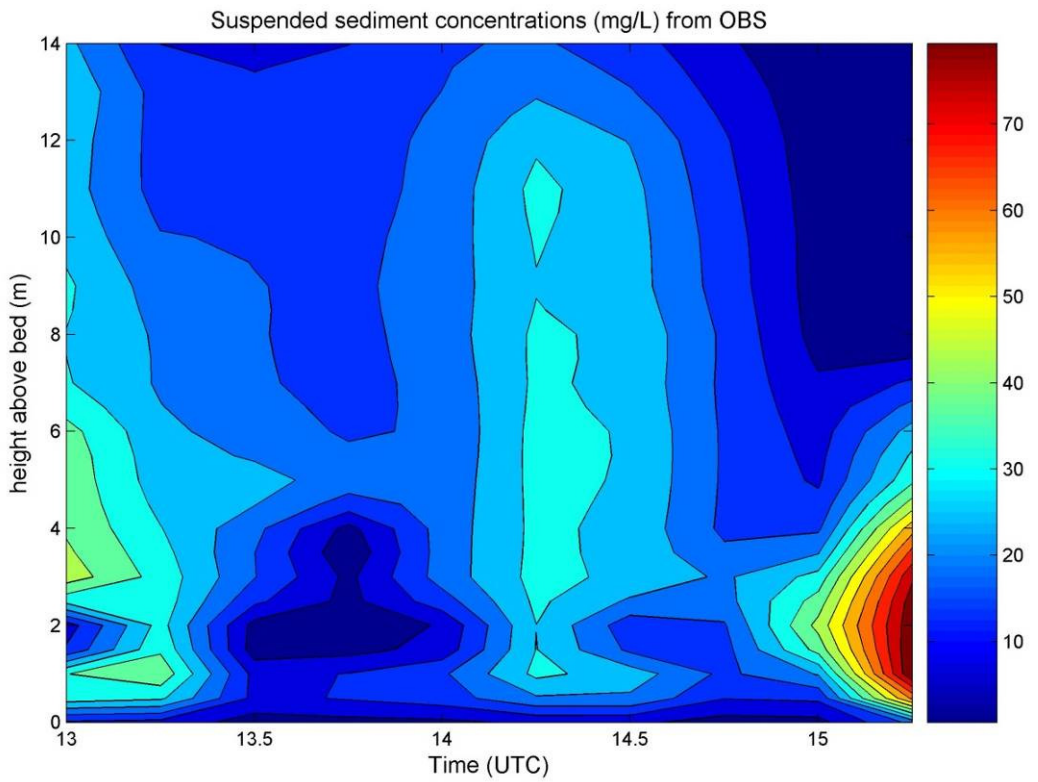


Figure 3.5: (A) Suspended sediment concentration in mg/L measured by the OBS and (B) Suspended sediment concentration in mg/L measured by the ADCP

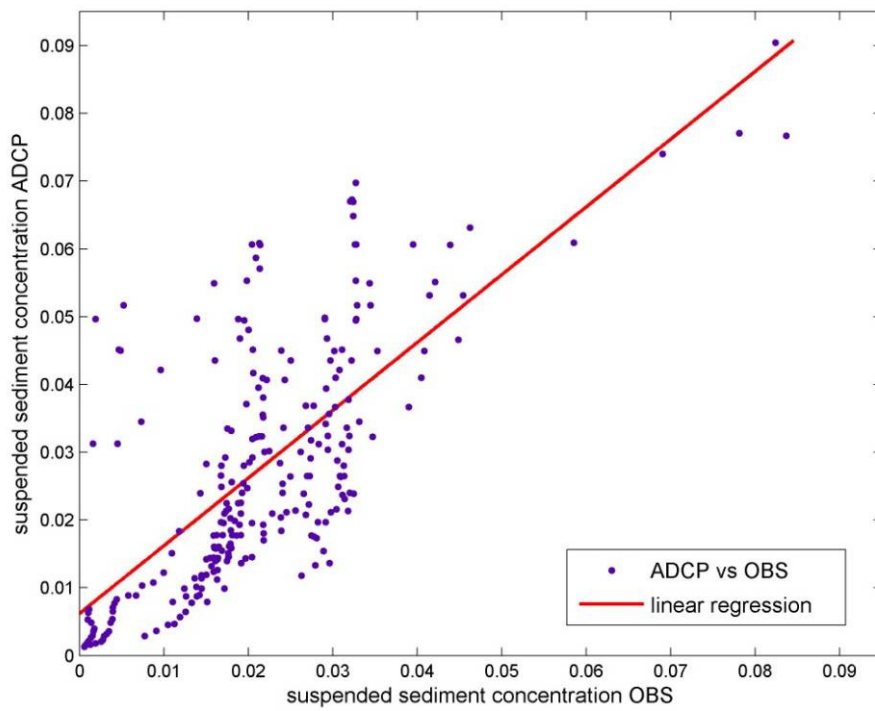


Figure 3.6: Linear regression between total suspended sediment derived from the ADCP and the suspended sediment concentration measured with the OBS during the calibration measurement.

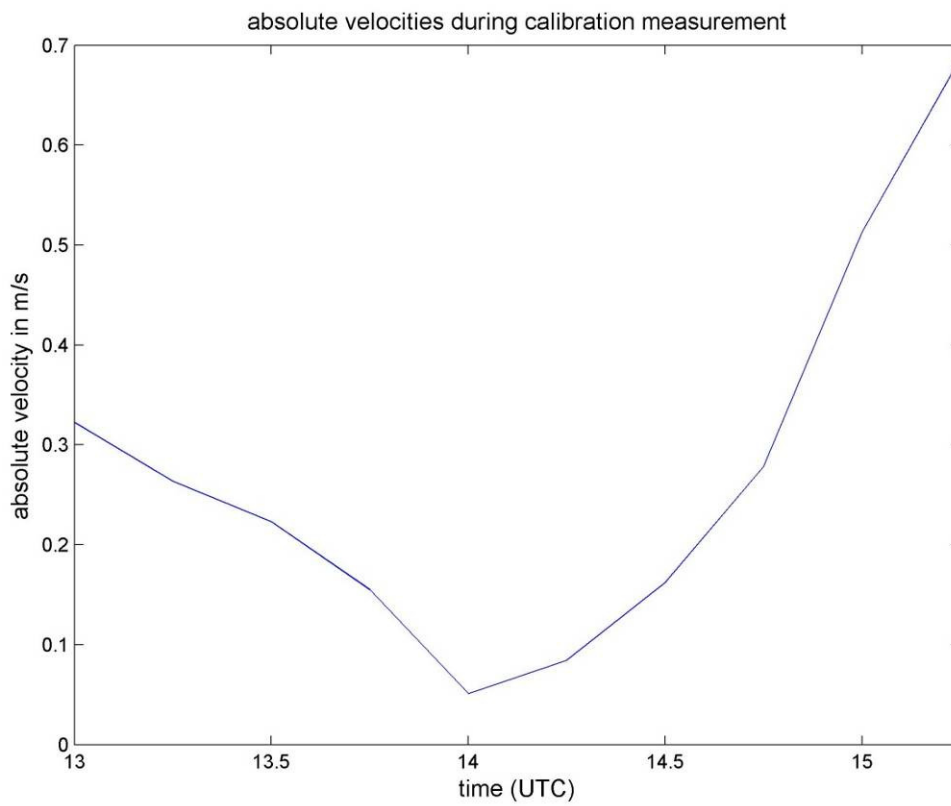


Figure 3.7: Absolute depth averaged velocities during the calibration measurement

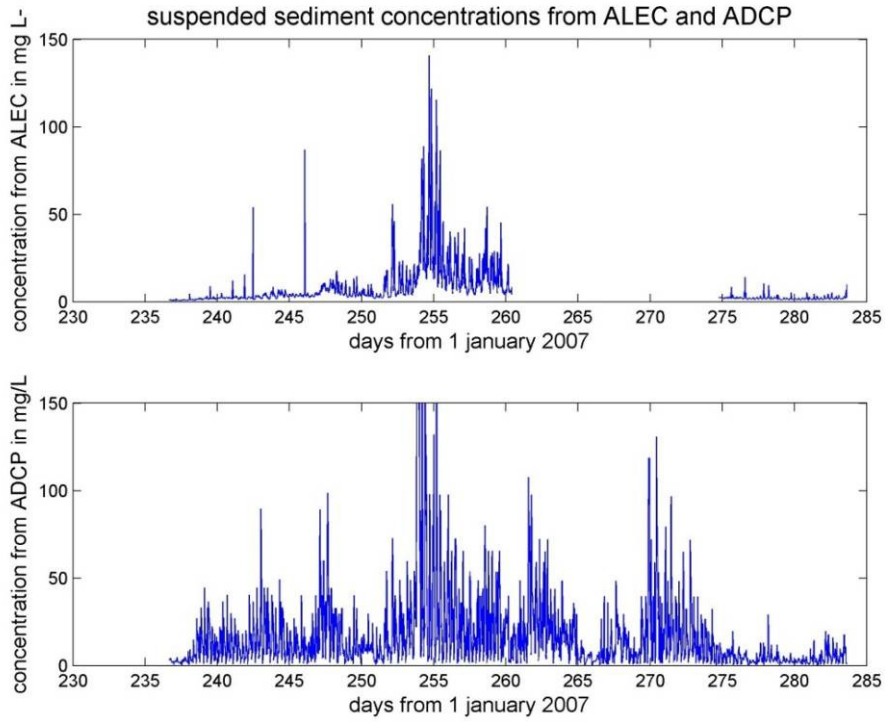


Figure 3.8: Concentration (mg/L) from ALEC in the top figure and concentration (mg/L) from the second lowest bin of the ADCP in the lower figure for $\gamma = 0.8$.

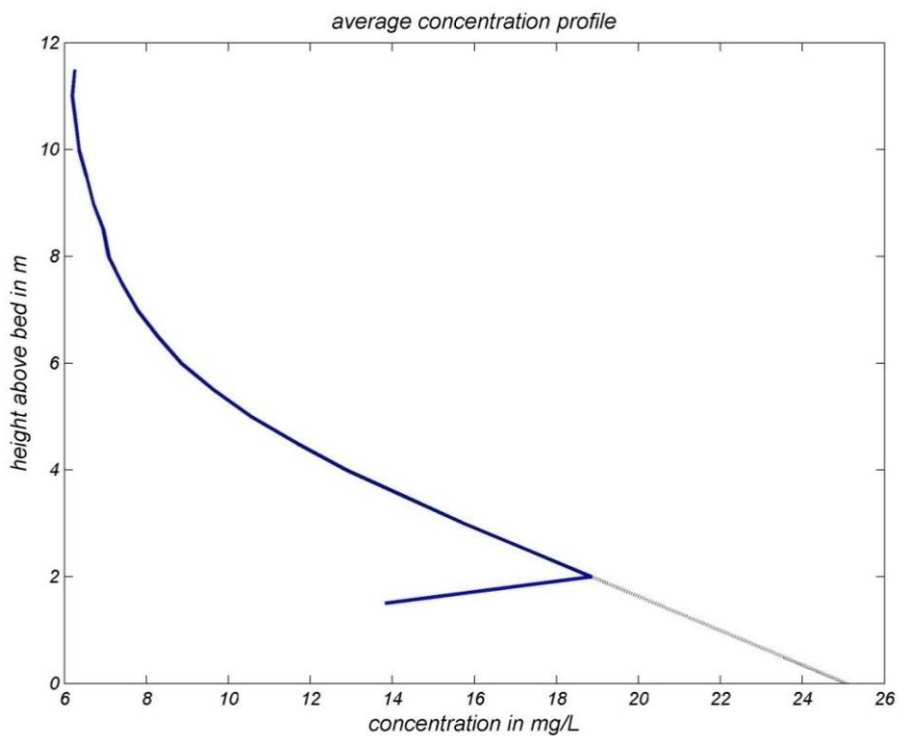


Figure 3.9: Mean concentration profile with the solid line representing the measured concentration and the dashed line the extrapolated concentration.

3.3 Indication of stratification

Turbulence in the water column is generated by winds, waves and tides. When wind velocity is large, wave height is large and currents are large, there will be large turbulent motions in the water column. Fresh river water which enters the North Sea will then be mixed with the saline water by the turbulence in the water. This will result in a vertical homogeneous water column.

When wind velocity is small, wave height is small and currents are small, the turbulence in the water column will be low. Fresh water entering the North Sea will float on top of the saline water. With low turbulent motion mixing of the water column will also be low and a stratified water column will develop.

Stratification inhibits turbulent motion. When two layers of water with different densities are on top of each other there will be no exchange of turbulent motion in the vertical (Simpson and Souza, 1995). So during periods of stratification there will be less turbulence and vertical mixing is reduced. This will influence the vertical velocity profile.

There were no direct measures of stratification, e.g. salinity differences over depth. However, an indication of stratification can be found in the tidal velocities. The tidal flow is not constant over depth, but has a vertical distribution. The velocity increases from the bottom on upwards and increases until it reaches a constant velocity. The velocities in the lower part of the water column are smaller due to friction and inertial forces (Marchuk and Kagan, 1984). This part of the water column is called the bottom boundary layer. Friction effects do not play a (large) role above this layer and the tidal velocities are constant in the vertical. The thickness of the bottom boundary layer can be calculated with:

$$\delta_l \cong \left(\frac{2\nu}{\sigma_0} \right)^{1/2} \quad (3.9)$$

With δ_l the thickness of the bottom boundary layer, ν kinematic viscosity of the fluid and σ_0 the oscillation frequency (Marchuk and Kagan, 1984).

The tidal movement of water can be decomposed in a clockwise and an anticlockwise circular movement. Both clockwise and anticlockwise component have a different bottom boundary layer thickness (Souza and Simpson, 1995). This is caused by a different oscillation frequency σ_0 due to the Coriolis frequency. The boundary layer thickness for clockwise motion is:

$$\delta_- = \left(\frac{2\nu}{(\omega - f)} \right)^{1/2} \quad (3.10)$$

The boundary layer for anticlockwise motion is:

$$\delta_+ = \left(\frac{2\nu}{(\omega + f)} \right)^{1/2} \quad (3.11)$$

In which ω is the frequency of the tidal constituent, ν is the eddy viscosity, which is assumed to be constant, and f the Coriolis parameter.

Simpson and Souza (1995) used Rhine ROFI values of $\nu = 1.2 \times 10^{-2} \text{ m}^2 \text{ s}^{-1}$, $f = 1.15 \times 10^{-4} \text{ s}^{-1}$ and $\omega = 1.41 \times 10^{-4} \text{ s}^{-1}$ can be used, resulting in: $\delta_- \approx 30 \text{ m}$ (clockwise component) and $\delta_+ \approx 10 \text{ m}$ (anticlockwise component; Simpson and Souza, 1995). Thus the clockwise boundary layer will cover the lowest 30 meter of the water column, while the anticlockwise boundary layer will only cover the lowest 10 meter of it (figure 3.10a). This means that the anticlockwise part will have no bottom friction effects above 10 meters above the bottom, while the clockwise part will have bottom friction effects until 30 meters above the bottom. Therefore the anticlockwise movement will be somewhat larger than the clockwise part and the tidal movement will be anticlockwise until 30 meters above the bed.

When fresh water flows on top of saline water, a shear plane will develop. Exchange of turbulent motions and transfer of momentum in the vertical are limited due to density differences (Simpson and Souza, 1995). Therefore water above this shear plane will not be distorted by frictional forces and acts like it is above the bottom boundary layer (figure 3.10b).

The effect on the clockwise component will be that the frictional forces will be restricted to the water column below this shear plane and therefore the clockwise tidal ellipse will be reduced below this shear plane. Above the shear plane the clockwise tidal ellipse will have free flow which is larger than the anticlockwise part. At the top the tidal movement will consist of a circular anticlockwise motion and a larger clockwise motion, which sums up to a clockwise ellipse. At the bottom the tidal movement will consist of a circular anticlockwise motion and a smaller clockwise motion, which sums up to an anticlockwise ellipse. Therefore the tidal ellipse at top of the water column becomes clockwise, while the tidal ellipse at the bottom becomes anti-clockwise (figure 3.10b).

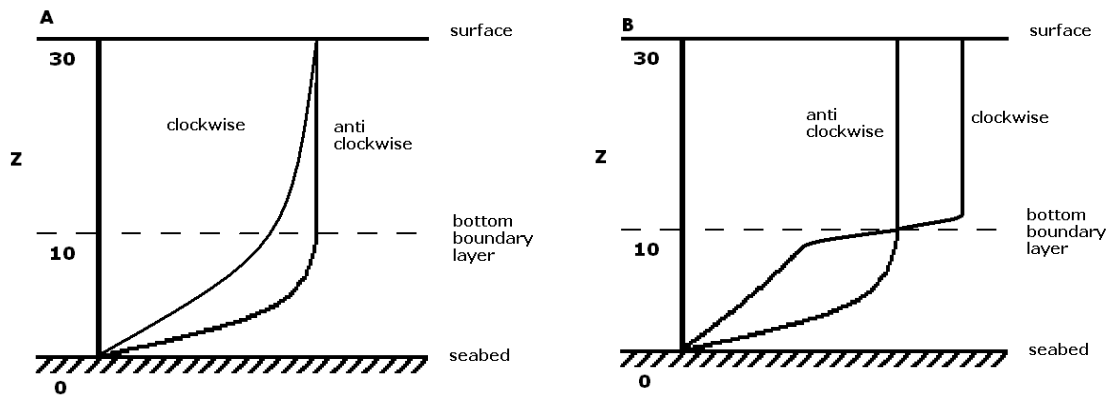


Figure 3.10: Bottom boundary layer with a) idealized situation and B) stratified situation, with shear plane at bottom boundary layer (Simpson and Souza, 1995).

3.4 Harmonic analysis

Tide is defined as the periodic movement which is directly related to some periodic geophysical force. The astronomical tide is the periodic movement related to movements in the earth-moon and earth-sun systems (Puch, 1987). The fundamental astronomical motions are summed up in table 3.1. Each motion has its period and frequency. Together these motions determine the tidal motion.

A lot of harmonics and linear combinations of the fundamental frequencies can be observed in tidal signals. The main tidal constituents and the astronomical motions of which the tidal constituents consist of are summed up in table 3.2.

The tidal motion differs at each location on earth. The water level elevation or current velocities over a period of time can be used to analyse the tidal motion at a specific site. When the site is at shallow water some additional constituents play a role. This is caused by additional friction and deformation of the tidal wave, which is absent in deep water. The additional constituents are called the shallow water constituents and consist of higher harmonics of the main constituents (table 3.3).

With harmonic analysis the tidal constituents can be extracted from the measured water level or tidal velocities. The tidal signal is modelled as the sum of different sinusoids. Each sinusoid represents an individual or a combination of astronomical forces and has the form $f(t) = H \cos(at + phi)$, in which $f(t)$ is the predicted tide at step t , H is the amplitude of the constituent, a is the angular speed of the constituent and phi is the phase of the constituent (Puch, 1987).

With a least squares fit the amplitude and phase of each tidal constituent is calculated. Error estimates are used to separate significant tidal constituents from insignificant tidal constituents at a specific site (Pawlowicz et al., 2002). Also the residual is calculated, the part that is not explained by the astronomical tide. This gives information on other

components like the meteorological effects on the water level. All calculations are done with Matlab, using T_Tide (Pawlowicz et al., 2002).

Tidal asymmetry is a factor that influences suspended sediment transport. Changes in relative phase and amplitude ratio between two constituents (e.g. between the M_2 -constituent and the corresponding shallow water tides M_4 , M_6 and M_8) can be related to the asymmetry of the tide. This will be used in calculating the suspended sediment transport processes (section 6).

Table 3.1: Basic tidal periods of astronomical motions (Puch, 1987)

Tidal period	Period (mean solar days/ Julian years)	Frequency (cycles per mean solar hour)	a (angular speed in degrees per mean solar hour)
T1: Mean solar day	1 MSD	1	15
T2: Mean lunar day	1.035 MSD	0.96613	14.49
s: Sidereal month	27.32 MSD	0.03660	0.549
h: Tropical year	365.24 MSD	0.00274	0.041
p: Moons perigee	8.85 Julian years	0.00021	0.046
N: Regression of moon's node	18.61 Julian years	0.00015	0.002

Table 3.2: Main tidal constituents (Puch, 1987)

Abbreviation	Composition	Character
O_1	T1 - s	diurnal tide
P_1	T1 + s - 2h	diurnal tide
K_1	T1 + s	diurnal tide
N_2	2T1 - s + p	semidiurnal tide
M_2	2T1	semidiurnal tide
L_2	2T1 + s - p	semidiurnal tide
S_2	2T1 + 2s + 2h	semidiurnal tide

Table 3.3: Shallow water constituents (Puch, 1987)

Abbreviation	Composition	Character
M_4	$2M_2$	fourth diurnal tide
M_6	$3M_2$	sixth diurnal tide
M_8	$4M_2$	eighth diurnal tide

4 Data:

4.1 Meteorological data

Wind data is available from a measurement station 10 km further offshore (figure 1.1). This data include wind direction and wind velocity at 20 meter above sea level. Wind data is available for the whole measurement period (Rijkswaterstaat).

There are some strong winds from the north-west during the measurement period, but the dominant wind direction during the measurement period is south-west (figure 4.1). South-western winds are also the dominant wind direction in the region according to literature (e.g. De Ruijter, 1992).

4.2 Wave data

Wave data is available from a wave buoy at the same position as the wind data (figure 1.1) Wave data include wave height, wave period and wave direction. Wave data is also available for the whole measurement period.

In general the waves are directed to the east with highest waves directed to the southeast. There are also smaller waves directed to the northeast (figure 4.2).

4.3 Salinity data

Salinity data at 1.5 meter above the bottom is not constant during the year. The maximum salinity measured is 32.85 psu on day 75 and the minimum salinity measured is 25.47 psu on day 77 (figure 4.3). The maximum difference in salinity within 1 M2 tidal cycle is 5.76 psu.

4.4 River discharge

Discharge data is collected near Lobith (Rijkswaterstaat). The mean discharge of the river Rhine in 2007 was 2375 m³/s (figure 4.3). The river discharge during in 2007 is characterized by flood peaks in February and March with a maximum discharge at day 65 of 6028 m³/s, a flood peak at the end of summer on day 226 of 4318 m³/s and a flood peak at the end of the winter on day 347 of 5365 m³/s.

wind directions in classes of 20 degrees and wind velocities in m/s

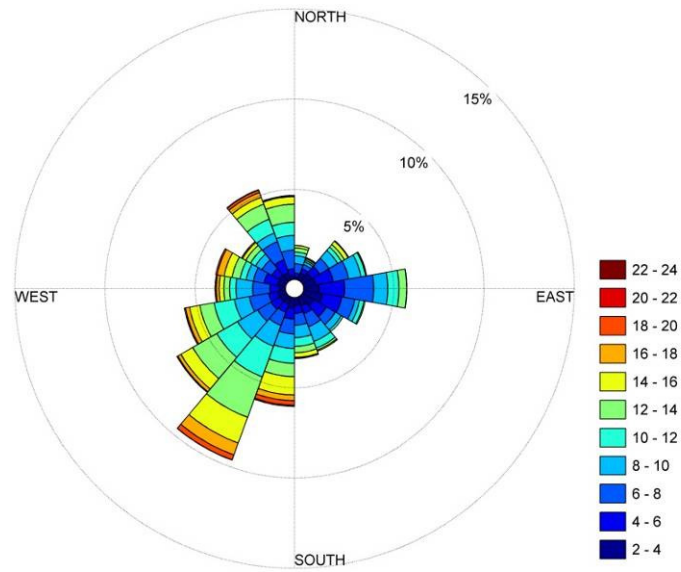


Figure 4.1: Wind direction and relative duration of the direction during ADCP deployment. Colours indicate the wind speed classes.

wave directions in classes of 20 degrees and wave height in meters

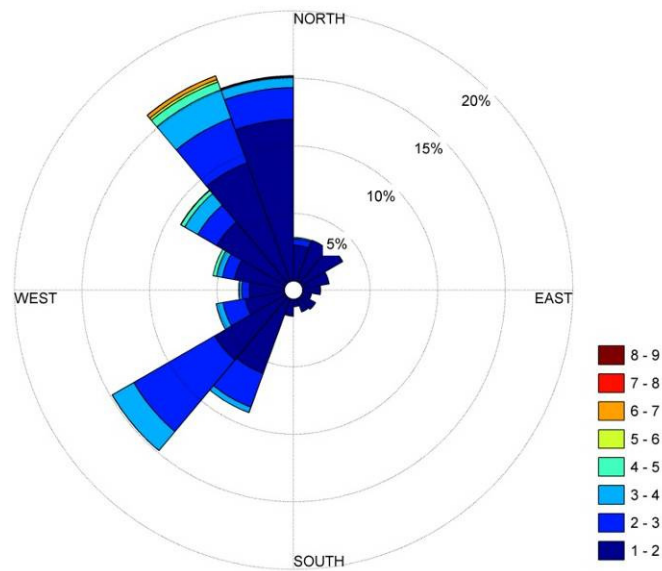


Figure 4.2: Wave direction and relative duration of the direction during ADCP deployment. Colours indicate the wave height classes.

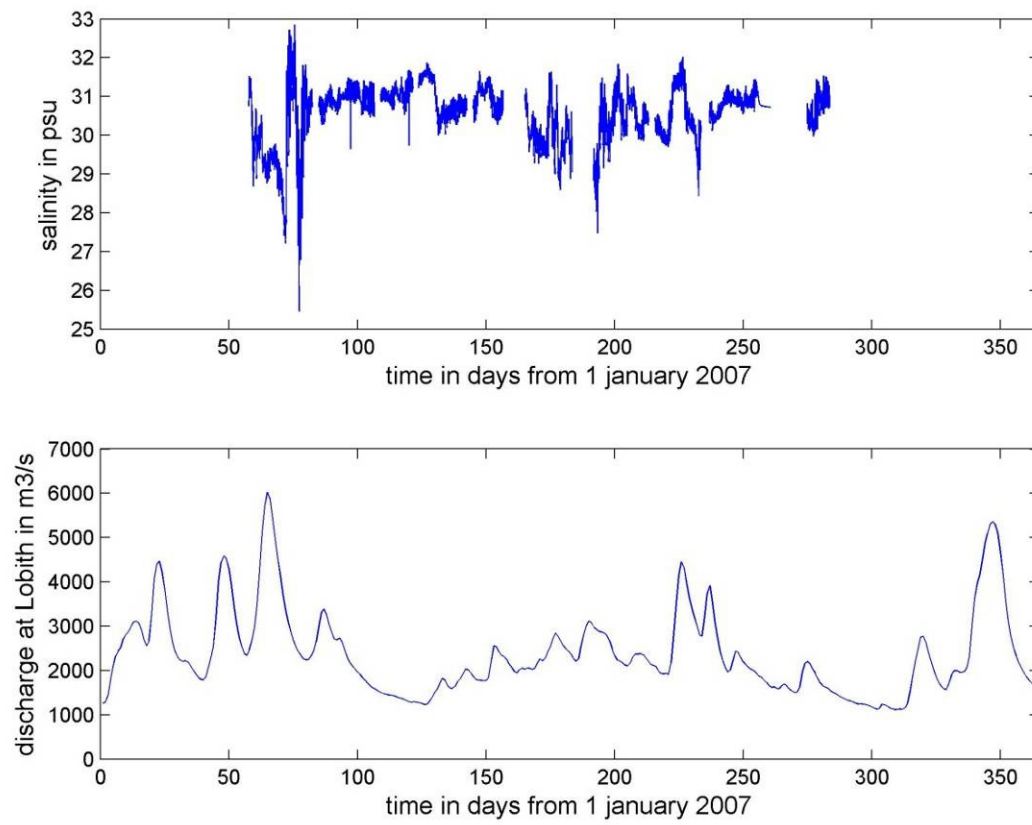


Figure 4.3: Salinity (psu) at 1.5 m above the seabed near the ADCP in 2007 (top) and river discharge at Lobith in m³/s in 2007.

5. Hydrodynamics

Velocities are measured by the ADCP in northern and eastern direction. The maximum flow velocities are directed along coast, with an angle of 17 degrees from the north. Ebb and flood velocities can be determined from this (table 5.1).

Table 5.1: Measured velocities in which positive values indicate an alongshore current to the north and a cross-shore current to the east (towards the coast).

Velocity	Along coast		Coast normal	
Maximum	1.30	m/s	0.39	m/s
Minimum	-1.11	m/s	-0.54	m/s
Depth average maximum	0.87	m/s	0.25	m/s
Depth averaged minimum	-0.77	m/s	-0.31	m/s
Depth average total	0.021	m/s	-2.1*10 ⁻⁴	m/s

The depth averaged alongshore current, averaged over the period between the first neap tide and the last neap tide from the measurement period, is 2.1 cm/s. This is somewhat lower than the time averaged velocities along the Dutch coast found in literature ranging from 3 cm/s to 15 cm/s (e.g. Simpson, 1997).

The net depth averaged current in the cross-shore direction, averaged over the same period as the alongshore current, is 2.7*10⁻⁴ m/s to the west, offshore. The net depth averaged water transport in cross-shore direction is close to zero, because there is a balance between onshore and offshore transport of water.

The time averaged cross-shore current has a strong variability over depth. There is a time averaged onshore current of 0.75 cm/s at 2 meter above the bottom and a time averaged offshore current of 1.5 cm/s near the top, at 12 meter above the bottom (figure 5.1).

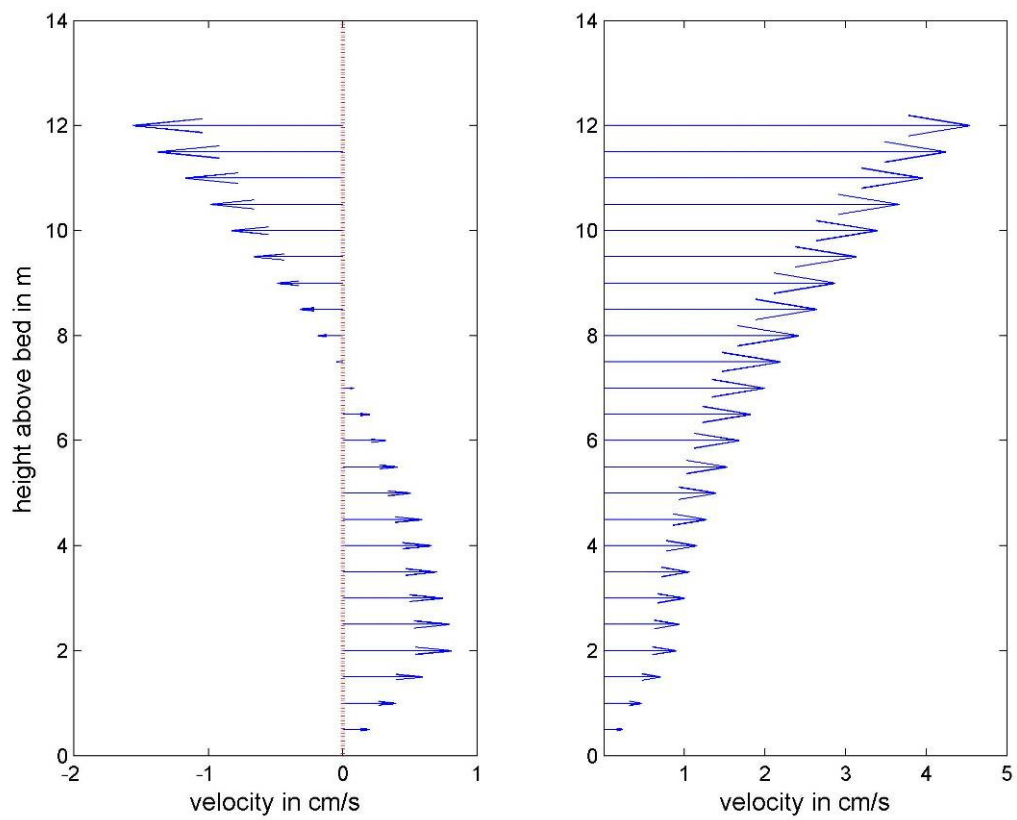


Figure 5.1: Cross-shore (left) and alongshore (right) time averaged current over the whole measurement period, 288 M2 tidal cycles, where velocities to the east (onshore) and north (alongshore) are positive and velocities to the west (offshore) and south (alongshore) are negative.

5.1 Tide

The direction of the current at the measurement location is for a large part determined by the tide. With harmonic analysis the main tidal constituents are determined for both the depth averaged alongshore velocities and the depth averaged cross-shore velocities over the measurement period (table 5.2 & 5.3). The tidal constituents determine 90.0% of the alongshore velocities, but only 24% of the cross-shore velocities.

This low correlation between the measured current and the predicted current is caused by large differences in measured current amplitudes through time. Therefore a harmonic analysis with a walking average of 25 hours is performed at each measured bin. The amplitude, phase and r^2 are calculated for every time step. The r^2 is plotted in figure 5.2. When r^2 reaches the value of 1, the currents are determined by the tidal constituents, when r^2 is low, the currents will also be influenced by other processes than the tide. In the cross-shore direction there are periods when the tide determines more than 95 percent of the current pattern, while at other moments during the measurement period the tide determines less than 80 percent of the tidal movement.

correlation between measured and predicted tide in cross-shore (left) and alongshore (right) direction

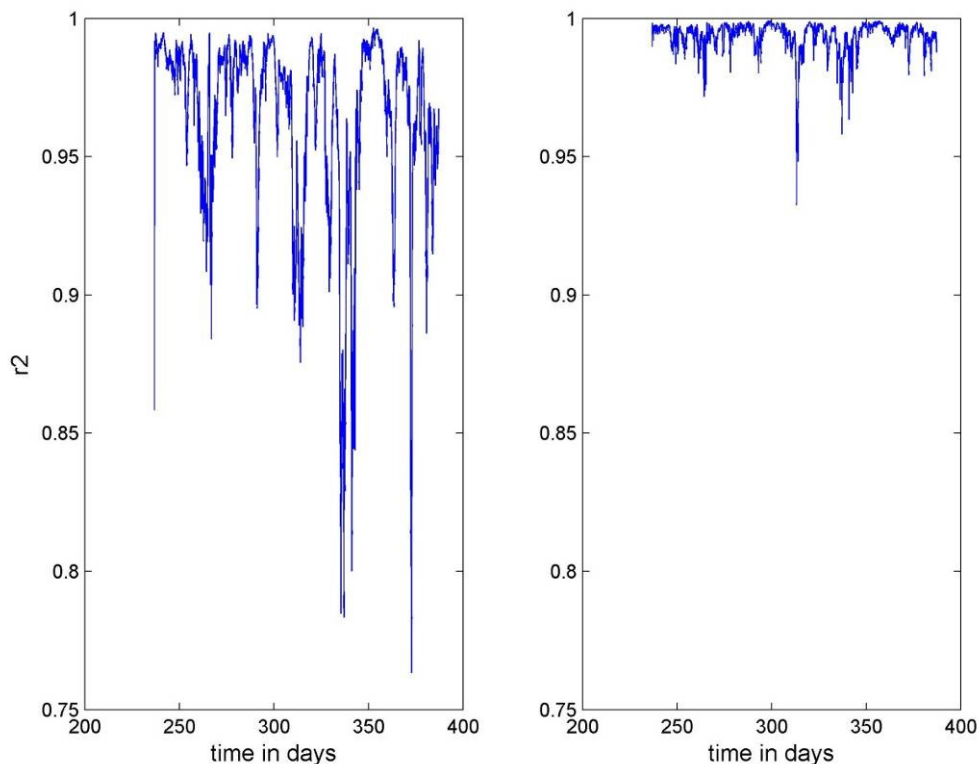


Figure 5.2: the correlation (r^2) between the measured velocities and the predicted tide with the M1, M2, M4, M6 and M8 tidal constituent.

Along the Dutch coast the M2 tidal cycle is dominant. The tidal amplitude is largest for the M2 tidal constituent and determines most of the tidal movement (table 5.2 & 5.3).

During flood the velocities are higher than during ebb, but the ebb period lasts slightly longer (figure 5.4). This is caused by the M2 tide and the corresponding shallow water tides M4, M6 and M8. The sum of the M2, M4, M6 and M8 tide with a phase lag between those tides results on day 237 in a flood tide of 0.564 m/s and an ebb tide of 0.471 m/s (figure 5.4). The flood tide lasts 5.9 hours and the ebb tide lasts 6.5 hours.

Due to bottom friction the velocities are higher in the top of the water column than near the bottom (figure 5.1). The cross-shore velocities are relative small.

At the measurement site there is a spring-neap tidal cycle (figure 5.3). This is caused by the combination of the M2 and S2 tidal constituent, which results in maximum flood velocities of 0.86 m/s during spring tide and 0.25 m/s during neap tide. The S2 tidal cycle is not used for the harmonic analysis, as it is only significant on time scales larger than the spring-neap tidal cycle, which is approximately 14 days.

Table 5.2: Main tidal constituents of the depth averaged alongshore velocities over the whole measurement period ($r^2=0.90$)

Tide	Frequency (day ⁻¹)	Amplitude (m/s)	Phase (degrees)
M1	0,0402	0,0029	88,6
M2	0,0805	0,510	18,5
M4	0,1610	0,044	59,1
M6	0,2415	0,032	352,8
M8	0,3220	0,011	31,6

Table 5.3: Main tidal constituents of the depth averaged cross-shore velocities over the whole measurement period ($r^2=0.24$)

Tide	Frequency (day ⁻¹)	Amplitude (m/s)	Phase (degrees)
M1	0.0402	0,0017	81,3
M2	0,0805	0,0024	61,7
M4	0,1610	0,015	354,6
M6	0,2415	0,0043	330,0
M8	0,3220	0,0039	290,3

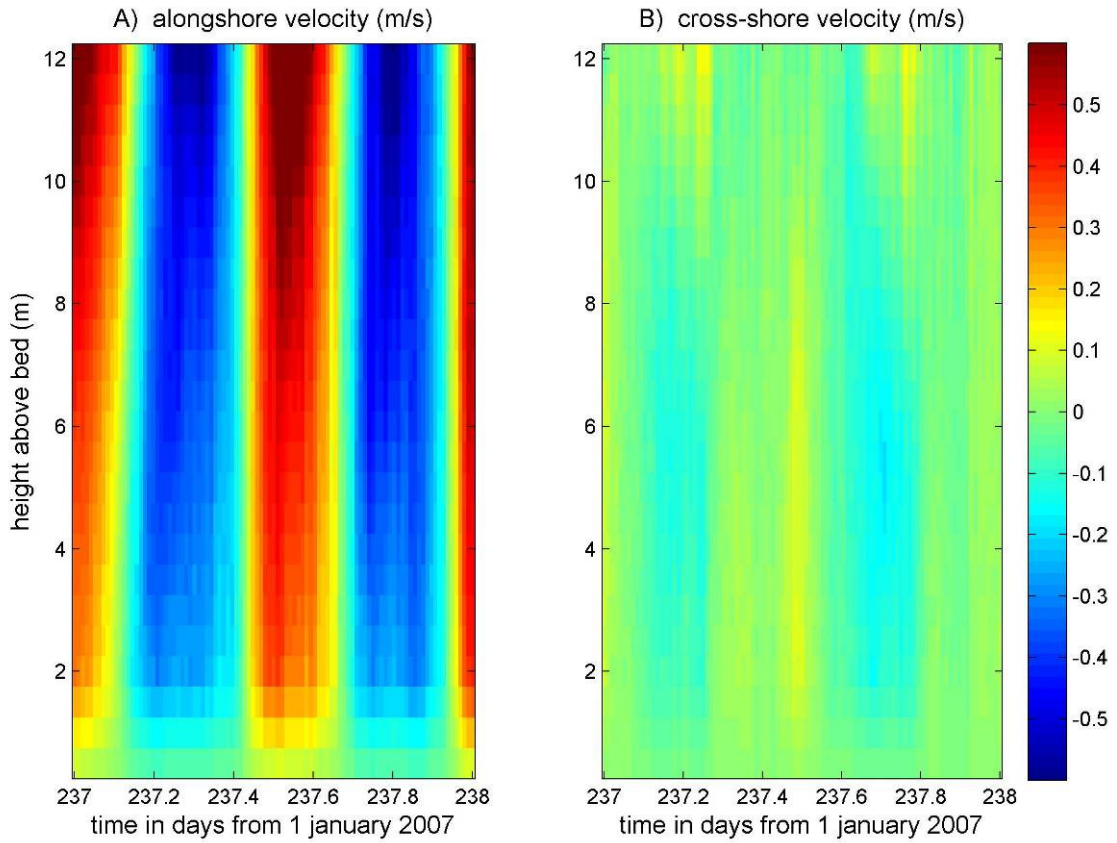


Figure 5.3: Measured (a) alongshore and (b) cross-shore velocities over depth during 2 M2 tidal cycles on day 237.

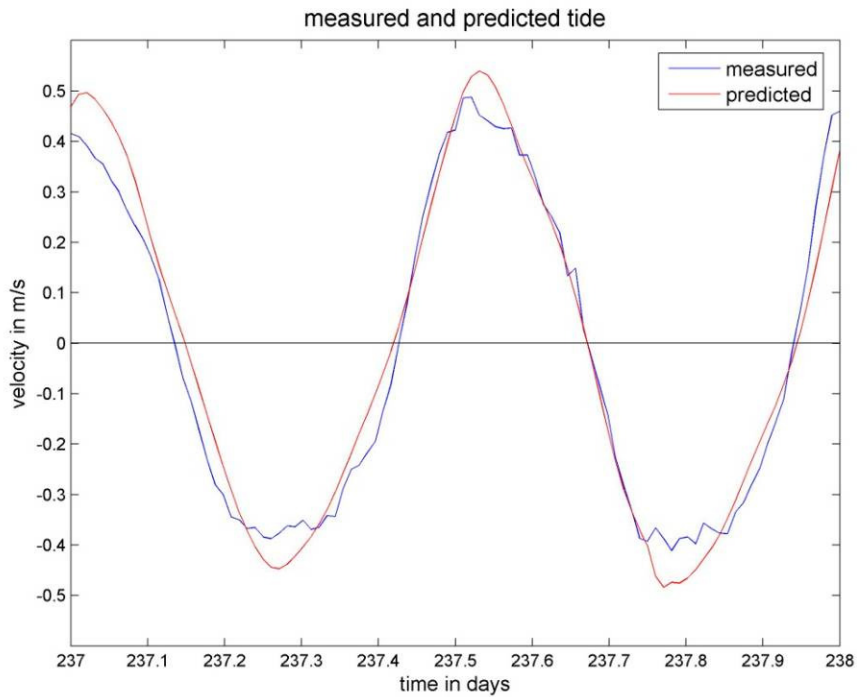


Figure 5.4: The tidal prediction on day 237 from the M1, M2, M4 M6 and M8 constituent. Positive values indicate flood, negative values indicate ebb.

5.2 Residual current

The residual current is the average flow over a tidal cycle or a longer time period. The residual flow is important for the suspended sediment transport (Van Leussen, 1991). Therefore the residual current is calculated, in both cross-shore and alongshore direction, and processes generating this residual current are examined.

The residual depth averaged current over the whole measurement period is approximately 2.1 cm/s in the alongshore direction to the north. The residual depth averaged current over each 25 hours is calculated for the whole measurement period. There is a large difference in the tidal averaged alongshore current through time (figure 5.5). The depth averaged residual current in the cross-shore is much lower than in the alongshore. But there are large differences over depth (figure 5.1). The residual current in the cross-shore is directed onshore near the bottom and offshore near the surface. The strength of the opposing currents is also varying with time (figure 5.6). There are periods when the currents in the cross-shore direction are opposing and periods when there is hardly any difference between the cross-shore current in the top and bottom of the water column.

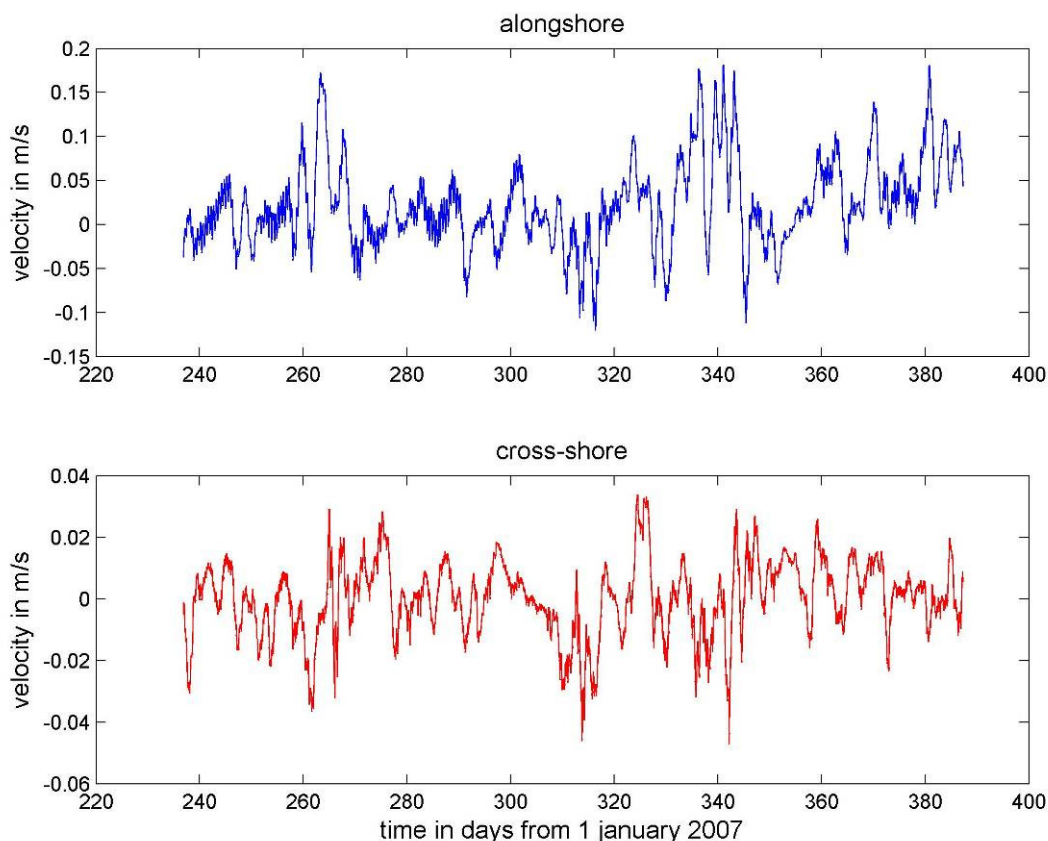


Figure 5.5: The residual depth averaged current over 25 hours, two M2 tidal cycles, during the whole measurement period for the alongshore current (top figure) and the cross-shore current (bottom figure).

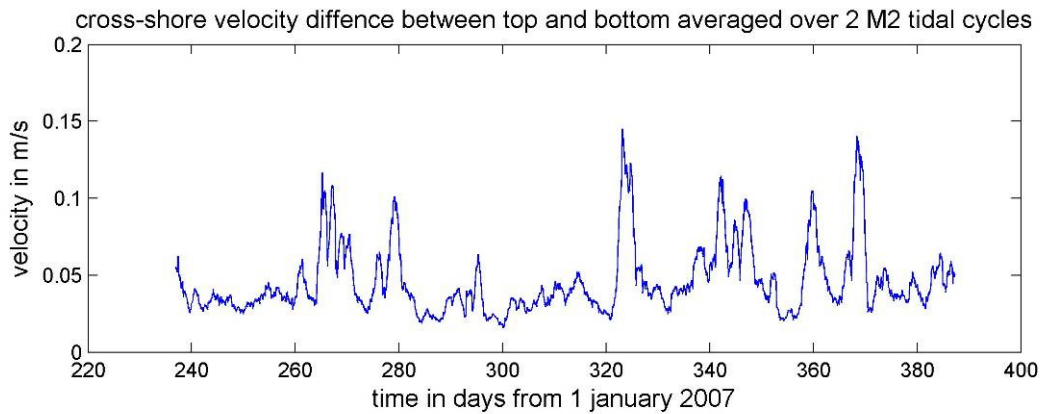


Figure 5.6: The difference between top and bottom velocity in the cross-shore direction, averaged at each time step over two M2 tidal cycles during the whole measurement period.

The residual current is either caused by the tide, wind or buoyancy driven processes. It is important to know what processes are dominant in this region, as by explaining the residual current, also the residual suspended sediment transport can be explained. Therefore the influence of wind and fresh water will be discussed below on both the alongshore and cross-shore residual current.

5.2.1 Wind effects on the residual current

During south-western and south-eastern winds the alongshore residual current is directed north and larger than the residual current averaged over the whole measurement period (figure 5.7a,c&d). During northern winds, the residual current is south directed (figure 5.7b&e). These results are similar to the results found by De Ruijter et al. (1987) for the residual currents at a site near Noordwijk, except that they found higher velocities as they only used currents under strong wind conditions (4 to 5 Bf).

The variability in residual current over depth in the cross-shore is visible in figure 5.7. The current near the bottom is directed onshore and the current near the surface offshore. These current directions persist under all wind directions. So the cross-shore circulation seems not to be dependent on the wind direction.

Wind stresses are possible to generate the residual current, but wind stresses do not cause the difference in current direction in the cross-shore between top and bottom layer of the water column, as these differences are independent of wind direction. The difference in current direction in the cross-shore between top and bottom layer of the water column could be caused by buoyancy driven circulation. Therefore periods when this current structure is seen, will be further analysed.

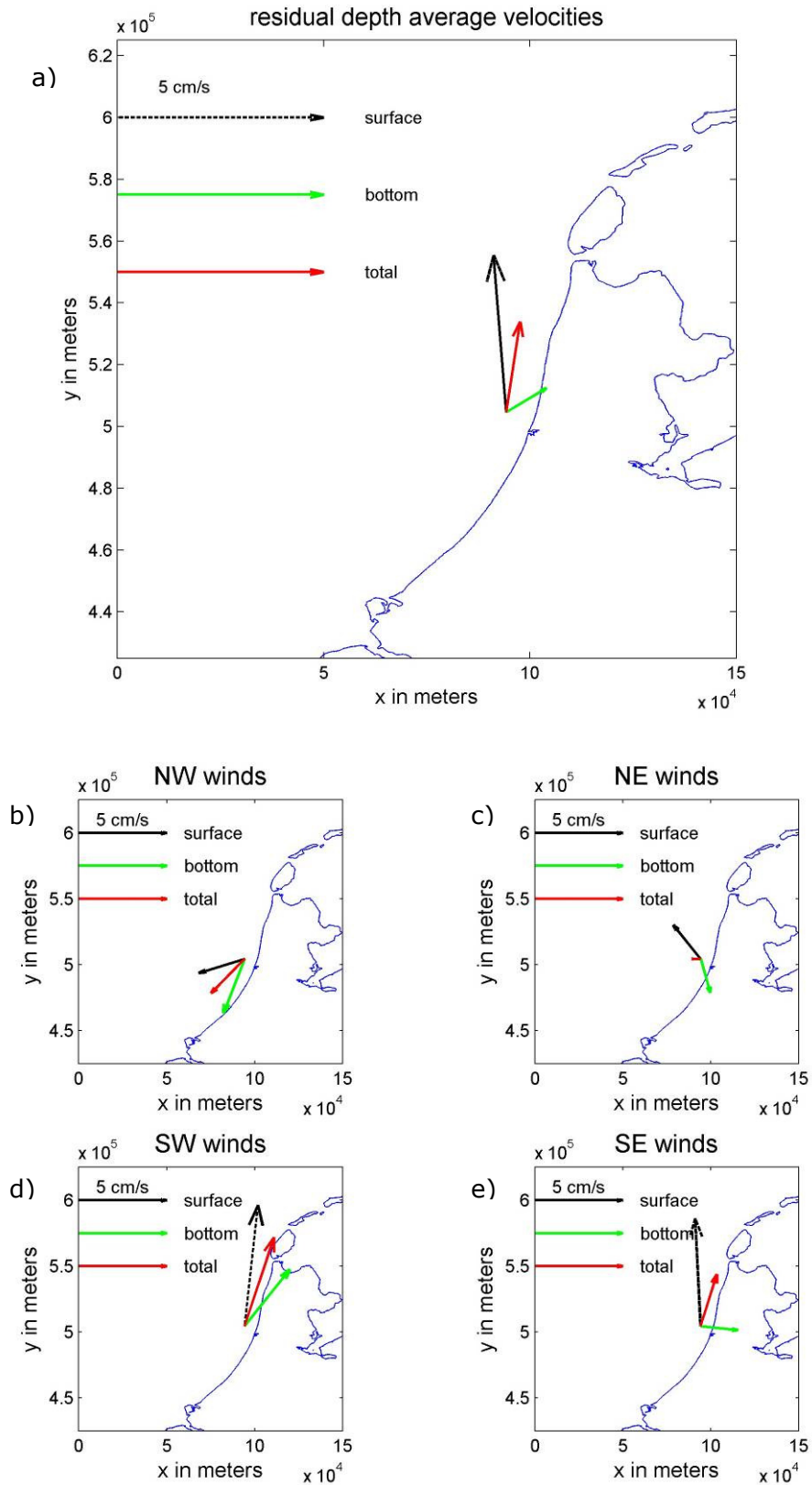


Figure 5.7: Residual depth averaged velocities, with a) averaged over total measurement period and b-e) averaged over periods with dominant wind direction.

5.2.2 Buoyancy effects on the residual current

There are no direct measures of the density difference over depth during the measurement period. Salinity is a good indication for stratification, but these measurements were not done during the measurement period. Therefore the tidal velocities are used as an indication of stratification.

The influence of fresh water can be indicated by examining the tidal ellipses (Simpson and Souza, 1995). The elliptical movement of the current during a tidal cycle can be made visible by plotting the velocities in alongshore direction versus cross-shore direction. This is shown for one tidal cycle on 20 November 2007 (figure 5.8). An ellipse is visible both in the top of the water column and at the bottom of the water column. At the top of the water column, the tidal ellipse is in clockwise direction, while at the bottom, the ellipse is anti-clockwise directed.

For the whole measurement period the M2 tidal ellipse properties are calculated with a walking average of 25 hours, which include minor and major axis, orientation, amplitude and phase. The ellipticity, ϵ , is calculated as a factor of major and minor axis, with 1 being a perfect circle and 0 a line, which indicated a minor axis of 0 with no tidal movement in the cross-shore. Negative values indicate a clockwise rotation of the tidal ellipse and positive values indicate an anticlockwise rotation (figure 5.9). When the tidal ellipse at the surface is rotating opposite of the ellipse at the bottom, this could be an indication of stratification of the water column as proposed by Simpson and Souza (1995).

Periods with small differences in the ellipticity between top and bottom layer are alternating periods with large differences (figure 5.9). The ellipticity near the bottom is around 0.3 during the periods with large differences, while at the surface the ellipticity is around -0.3. The periods with large differences last for a few days. There were eight periods with large ellipticity differences between top and bottom during the measurement period.

The ellipticity difference is the difference in ellipticity between the bottom and the near surface layer (figure 5.10a). The vertical lines in figure 5.10 show the maximum ellipticity differences during periods when ellipticity differences between top and bottom of the water column exceeded 0.2.

The peaks in ellipticity coincide with large difference of residual current in cross-shore direction between top and bottom of the water column (figure 5.10b & 5.12). When ellipticity differences between top and bottom of the water column are large, the current direction between top and bottom layer in the cross-shore direction is opposite. The

correlation between ellipticity differences and cross-shore current differences has an r^2 of 0.68 (figure 5.11).

When tidal current amplitudes are small, around neap, the highest differences in tidal ellipses between top and bottom layer of the water column are observed. The differences are much smaller when tidal current amplitudes are large.

This is not true for the periods around day 250, 310 and 340, when tidal current amplitudes were small, but no large differences in tidal ellipse are visible. Around day 360 there is a large difference ellipticity between top and bottom of the water column, while tidal current amplitudes were large. For these periods not the spring/neap cycle, but other process determine the ellipticity.

Wind stresses and wave activity can also be compared to the ellipticity (figure 5.10d&e). When wind velocity is large and wave height is large, there are no large differences in tidal ellipses. Around day 250, 310 and 340 the wind velocity was large and the wave height was large and thus mixing of the water column was also large. This could explain why there are hardly differences in tidal ellipse properties, even though the tidal current amplitudes were low.

The period of large differences in ellipticity between top and bottom of the water column around day 360 is more difficult to explain, as tidal velocities were large and wave activity was moderate. It is possible that this period can be explained by a flood wave from the river Rhine.

There was a flood wave near Lobith around day 342 (figure 5.10f). A flood wave of the river takes about 2 days to travel from the German border to the North Sea basin (Terwindt, 1967). The transport of the buoyant water mass along the Dutch coast takes more time, in the order of a few weeks. Therefore this flood wave is a possible explanation for the differences in tidal ellipse properties of bottom and surface water around day 360.

The residual current along the coast to the north from day 344 to day 360 was 4.2 cm/s. The total distance travelled by a water mass in 16 days would be 58 km. As the measurement location is approximately 70 north of the outflow point of the river Rhine, it is reasonable that the flood wave on day 342 at Lobith would have reached the measurement location on day 360.

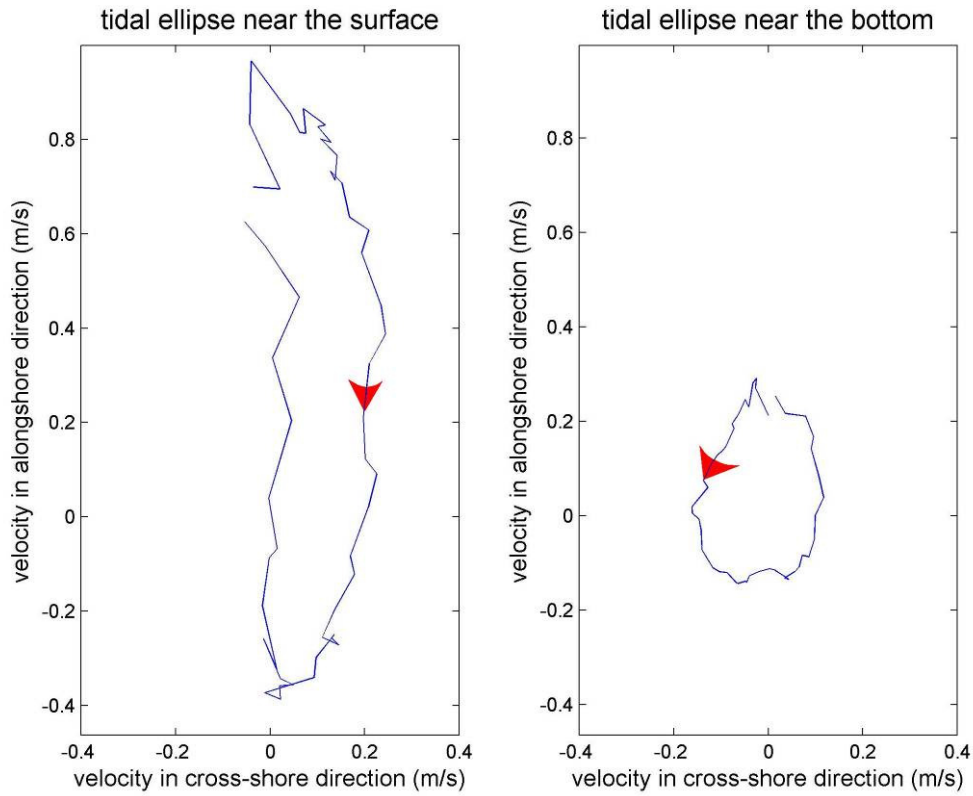


Figure 5.8: Tidal ellipses near the bottom and near the surface for 1 M2 tidal cycle on day 323. The red arrow indicates the direction of the tidal ellipse.

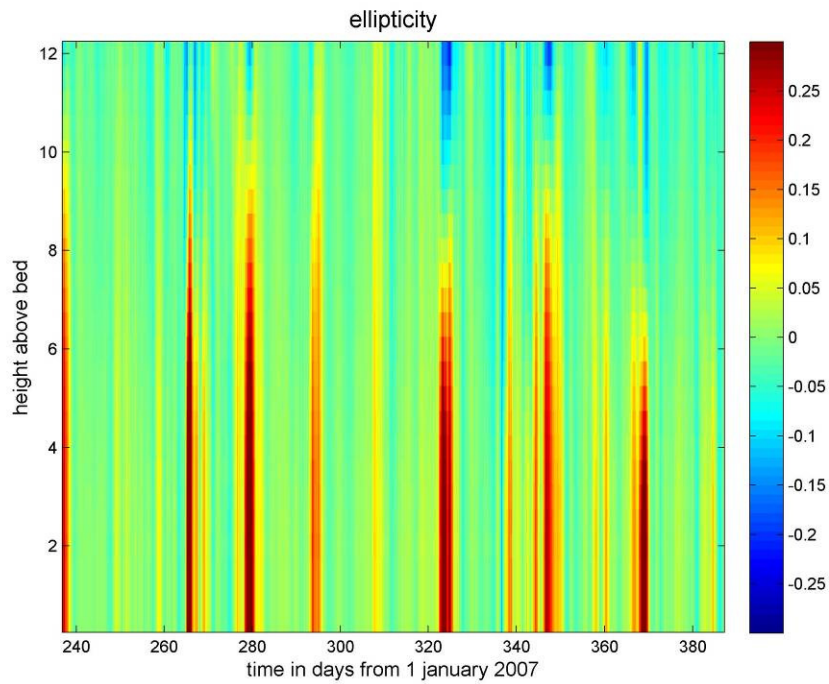


Figure 5.9: Ellipticity during the measurement period with negative values indicating clockwise motion and positive values anticlockwise motion.

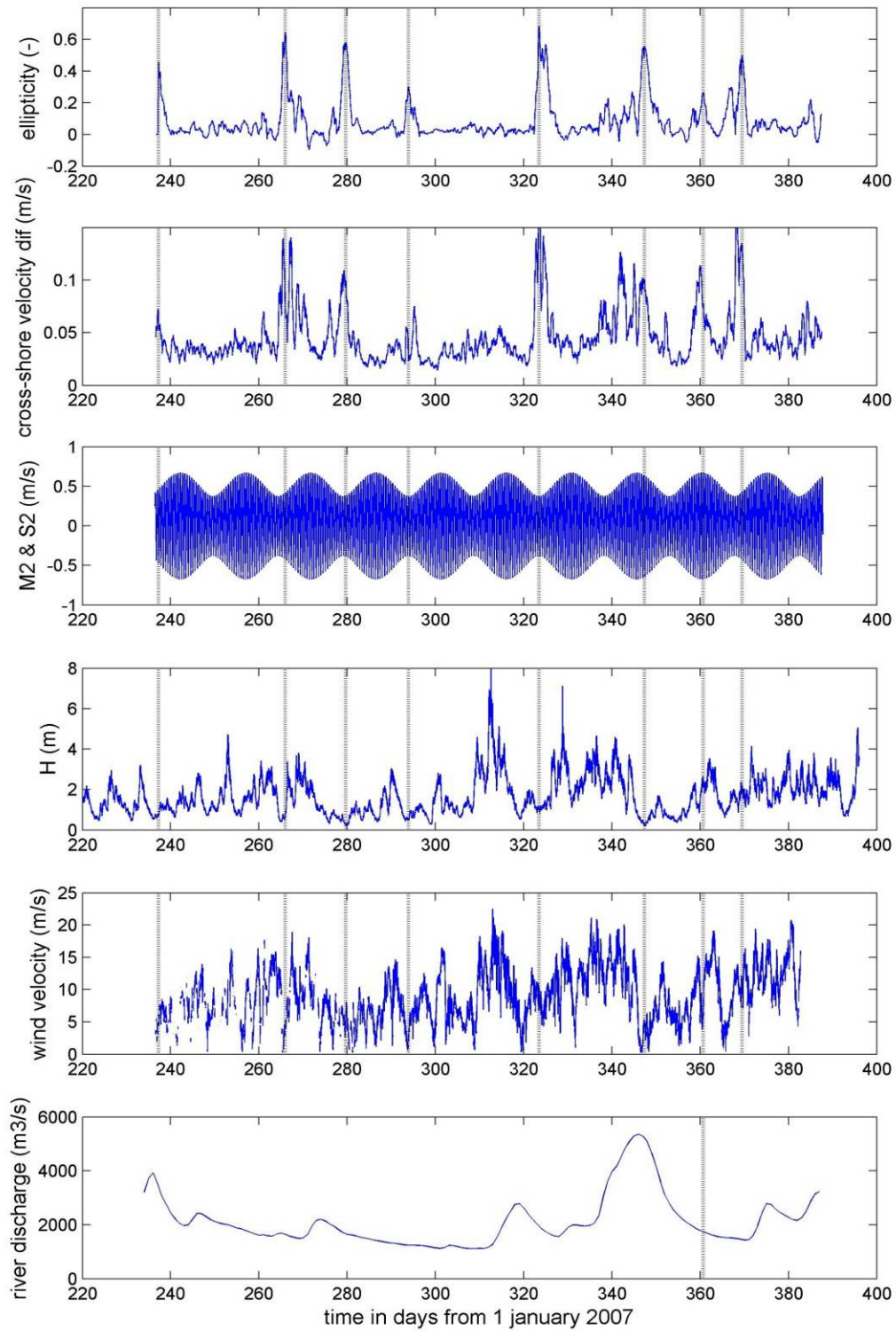


Figure 5.10: a) Ellipticity difference between bottom (2 meter above the seabed) and top (2 meter from the surface) (-), b) Absolute difference in residual cross-shore velocity between top and bottom (m/s), c) Alongshore M2 and S2 current amplitudes (m/s), d) Wave height (m), e) wind velocity (m/s) and f) River discharge near Lobith (m³/s). Vertical lines indicate peaks in ellipticity.

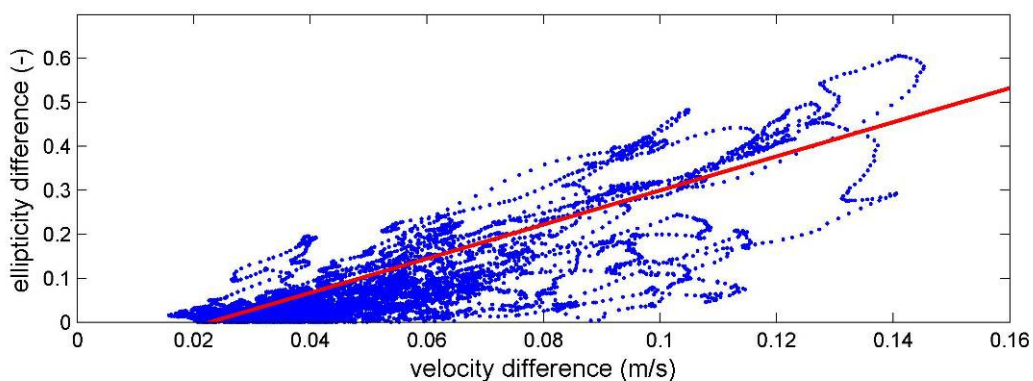


Figure 5.11: Correlation between the ellipticity difference in the top and bottom of the water column and the velocity difference in the cross-shore direction in the top and bottom of the water column. Both velocity difference and ellipticity are averaged over two M2 tidal cycles. The r^2 is 0.68.

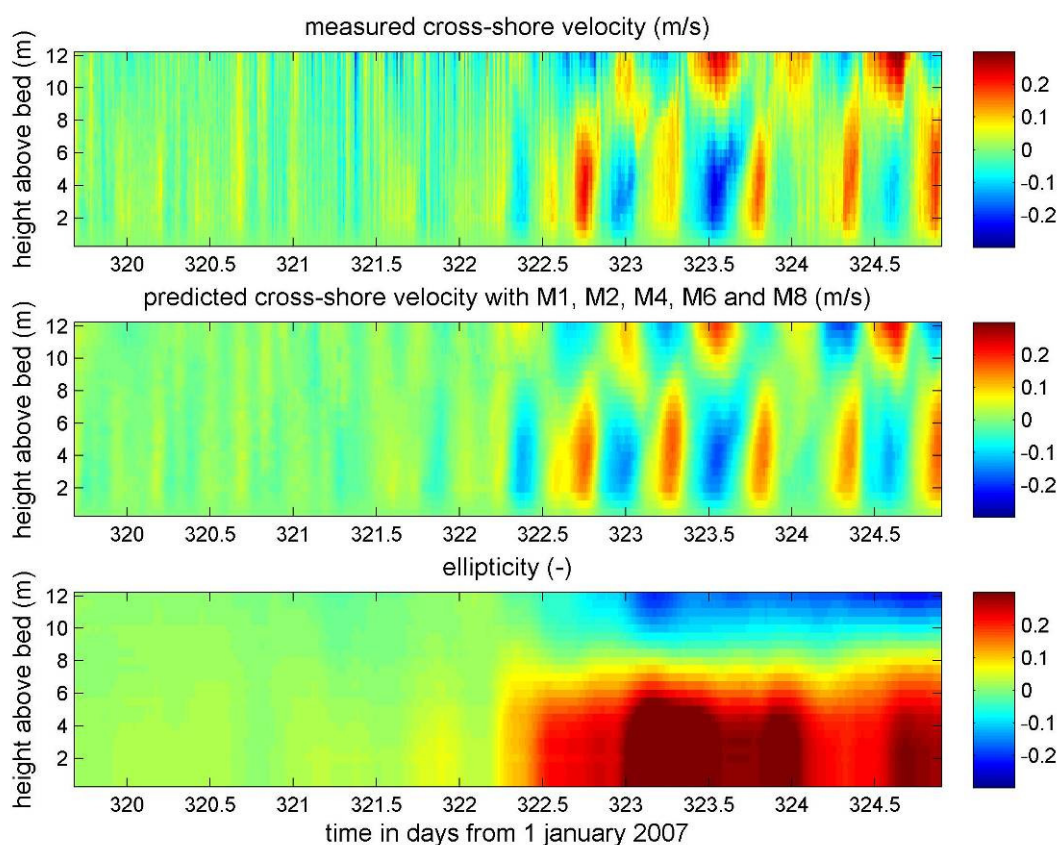


Figure 5.12: Velocities in cross-shore direction with positive values directed onshore (top), predicted velocities with the M1, M2, M4, M6 and M8 tidal constituent (middle) and ellipticity (bottom). The results are shown for a 4 day period with changing tidal ellipse properties.

6. Suspended sediment

The suspended sediment concentration for the whole measurement period is calculated with the calibrated ADCP data (figure 6.1). During the measurement period the maximum depth averaged suspended sediment concentration was 0.46 g/L. The lowest measured value is near 0 g/L (8.9×10^{-3} g/L). Short fluctuations are seen within one day, which could be associated with tidal currents. There are period with higher concentrations, lasting a few days to weeks, which could be associated with tidal processes, but also wind and wave driven processes.

To investigate the tidal influence on the concentration fluctuations, a harmonic analysis is performed on the concentration time series at all depths. The harmonic analysis is done for every 25h, two M2 tidal cycles, over the whole measurement period. From this harmonic analysis a reconstruction is made with the M1, M2, M4, M6 and the M8 tidal constituent, which are the dominant constituents, and the mean concentration.

The tidal signal is visible from day 320 to 325 (figure 6.2). The tidal prediction explains around 80 percent of the measured suspended sediment concentration during the measurement period (figure 6.3). So the variability of the suspended sediment concentration within one day can be for a large part explained by the tidal currents.

The bottom graph of figure 6.2 shows the mean concentration during the 5 days. This mean concentration was large during day 320, 321 and 322. In the last days of this period the mean concentration decreased. This trend is also seen in the measured concentrations. So the large fluctuations in suspended sediment concentration seen in figure 6.1 seem to be determined by the mean tide and not by tidal fluctuations. These could be related to other processes like waves and wind.

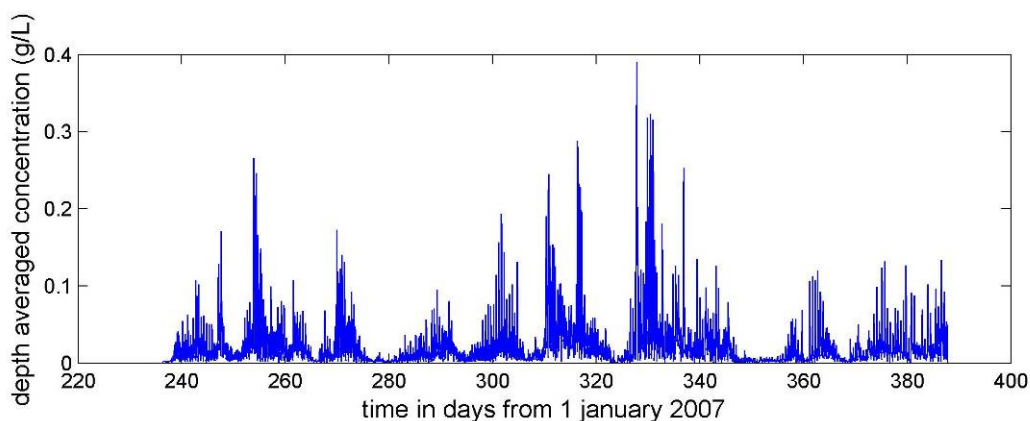


Figure 6.1: depth averaged suspended sediment concentration during the whole measurement period.

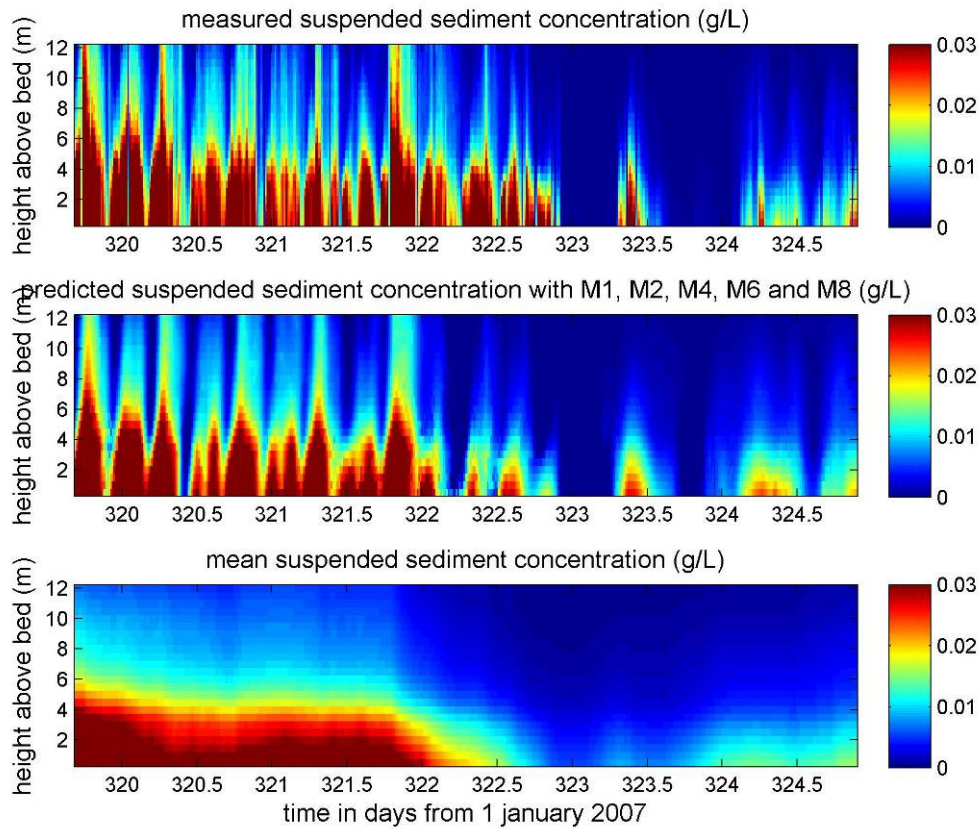


Figure 6.2: Measured suspended sediment concentration (top), predicted suspended sediment concentration with the M1, M2, M4, M6 and M8 tidal constituent (middle) and the mean suspended sediment concentration, calculated with a walking average over 2M2 tidal cycles (bottom). These plots were made from day 320 to 325.

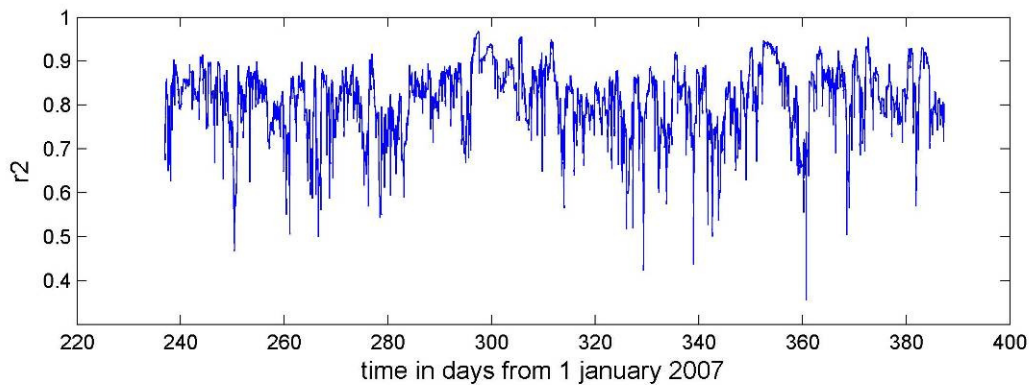


Figure 6.3: Correlation between measured depth averaged suspended sediment concentrations and predicted depth averaged suspended sediment concentration

When wave height is large, the suspended sediment concentration is large. When wave height is small, the suspended sediment concentration is low. A linear cross correlation between the tidally averaged suspended sediment concentration and tidally averaged wave height is performed in Matlab. This results in an r^2 of 0.55 over the whole measurement period (figure 6.4).

Sediment needs time to get resuspended as turbulence, induced by waves, increase in the water column. This is caused by the scour lag of sediment (Van Straaten and Kuenen, 1957). When turbulence induced by waves decrease, as a result of decreasing wave height, the suspended sediment does not settle immediately, but after a short period of time. This is called the settling lag (Van Straaten and Kuenen, 1957). A time lag between wave height and suspended sediment could increase the correlation between wave height and suspended sediment concentration.

However, when comparing the data over the whole measurement period, including a time lag does not make the relation more significant. There is hysteresis seen in figure 6.4, but the scour lag and the settling lag are not constant over the measurement period. At some moments the concentration increases directly with increasing wave height, at other moments it lasts a few hours. This is caused by several conditions, e.g. different bottom sediment, different storm periods and different tidal current amplitudes. When looking at separate events, the correlation between suspended sediment concentration and wave height could become better.

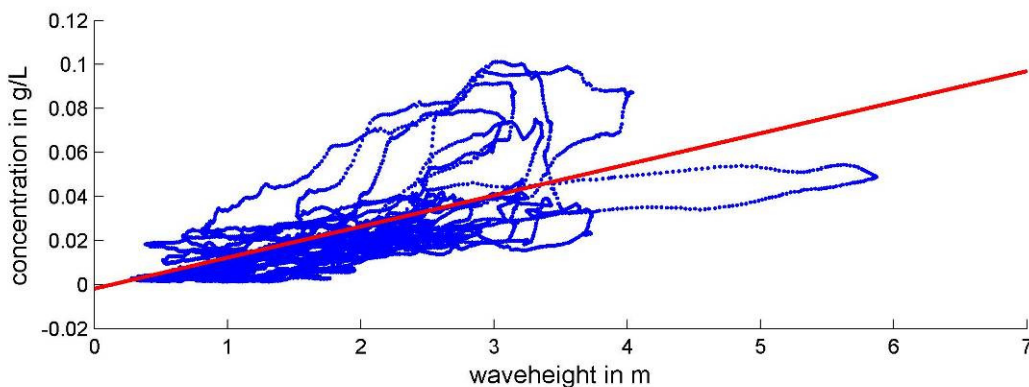


Figure 6.4: The wave height averaged over each 25 hours and the suspended sediment concentration averaged over each 25 hours. The red line indicates the linear correlation between the two parameters.

6.2 Suspended sediment transport

The transport of the suspended sediment is the velocity multiplied by the suspended sediment concentration integrated over each time period (equation 6.1).

$$\frac{1}{T} \int uc dt = \langle uc \rangle_{meas} \quad (\text{eq. 6.1})$$

In which u is the measured velocity and c the measured concentration. The transport can also be calculated as the sum of the mean suspended sediment transport and a fluctuating part of the suspended sediment transport (Kreeke et. al, 1997):

$$\langle uc \rangle_{pred} = \langle u \rangle \langle c \rangle + \langle (u - \langle u \rangle)(c - \langle c \rangle) \rangle \quad (\text{eq. 6.2})$$

In which the left hand side is the total measured suspended sediment concentration averaged over 25 hours, $\langle u \rangle * \langle c \rangle$ is the mean suspended sediment transport averaged over 25 hours and the last part of the right hand side is the fluctuating part of the suspended sediment transport, also averaged over 25 hours. This fluctuating part of the suspended sediment transport can be written as the sum of a harmonic series with tidal frequencies. The harmonic analysis of the tidal velocities and the concentrations is used for the calculation. The total transport can then be written as:

$$\begin{aligned} \langle uc \rangle_{pred} = \langle u \rangle \langle c \rangle &+ \left\langle \frac{1}{2} * U_{m1} C_{m1} * \cos(\varphi_{u,m1} - \varphi_{c,m1}) \right. \\ &+ \frac{1}{2} * U_{m2} C_{m2} * \cos(\varphi_{u,m2} - \varphi_{c,m2}) \\ &+ \dots + \left. \frac{1}{2} * U_{m8} C_{m8} * \cos(\varphi_{u,m8} - \varphi_{c,m8}) \right\rangle \end{aligned} \quad (\text{eq. 6.3})$$

With U and C being the amplitude of respectively the current and the suspended sediment concentration and φ_u and φ_c being the corresponding phase. The M1, M2, M4, M6 and M8 tidal constituent are used for the reconstruction of the suspended sediment transport.

The reconstruction is done for the alongshore transport and the cross-shore transport over the whole measurement period (figure 6.5 and 6.6). The measured (eq 6.1), the predicted (eq. 6.2), and the mean suspended sediment transport are separately calculated (first part right hand side of eq. 6.2) and the separate contributions of the M2 and M4 tidal constituent (second part right hand side of equation 6.2).

The difference between measured and predicted transport in the alongshore is small (figure 6.5c). In the alongshore the sum of the mean and M2 component of the suspended sediment transport determines most of the predicted suspended sediment transport (figure 6.5b). The predicted transport of the M4 tidal constituent is relative small.

The calculation of the M4 tidal constituent is a measure for the transport induced by the tidal asymmetry. Tidal asymmetry means that during ebb the concentrations and tidal velocities are higher or lower than during flood. This difference will generate a net transport during a tidal cycle. The transport generated by the M4 tidal constituent is directed north through the whole measurement period. This means that more sediment is transported towards the flood direction than in the ebb direction. However this transport is relative small compared to the mean transport and the transport generated by the M2 tidal constituent. This means that other processes are dominant for the suspended sediment transport in the alongshore during the measurement period.

The difference between the measured and predicted transport in the cross-shore is larger than in the alongshore (figure 6.6c). The tidal currents in the cross-shore were less good predicted, as the currents in the alongshore (figure 5.2). This will also cause the prediction of the suspended sediment transport to be less accurate in the cross-shore than in the alongshore. As a result also the transport induced by the M2 and M4 tidal component is relative small compared to the mean transport.

Tidal asymmetry plays a role in the suspended sediment transport in the cross-shore. The transport direction induced by the M4 tide in the cross-shore direction is in the offshore direction during most of the measurement period (figure 6.6f).

Tidal asymmetry is in the alongshore a small part of the total suspended sediment transport. The mean transport and the transport associated with the M2 tide determine most of the total transport. This transport is a combination of transport by the tide, wind and wave driven transport and transport induced by a buoyancy driven current.

Wind direction and magnitude determine the residual current along the Dutch coast (section 5), which imply that it can also determine the mean transport direction along the Dutch coast. When wind direction changes, also the residual current changes and the suspended sediment transport changes. The transport direction of the suspended sediment during northern winds is to the south (figure 6.7). When wind direction is south, the transport direction is to the north (figure 6.7).

The suspended sediment transport in the cross-shore is not directly related to wind direction (figure 6.7). With northern winds, the transport direction is directed offshore. With south-western winds, the transport direction can be both onshore and offshore. To investigate if tidal asymmetry determines the transport direction in the cross-shore, the

influence of the suspended sediment flux generated by the tidal asymmetry is compared to the residual flux:

$$D_{abs} = \frac{(|T_{res}| - |T_{asym}|)}{(|T_{res}| + |T_{asym}|)} \quad (\text{eq. 6.4})$$

With D_{abs} being the dominance of the suspended sediment flux generated by tidal asymmetry, where $D_{abs}=1$ indicates a dominance by the residual flux and $D_{abs}=-1$ indicated a dominance by the suspended sediment transport by tidal asymmetry. Whether the residual suspended sediment flux has the same orientation as the tidal asymmetry suspended sediment flux is calculated with the relative difference, in stead of the absolute difference:

$$D_{rel} = \frac{(T_{res} + T_{asym})}{(|T_{res}| + |T_{asym}|)} \quad (\text{eq. 6.5})$$

With D_{rel} being the relative direction of the two fluxes, 1 indicates both fluxes to the north, -1 indicates both fluxes to the south and 0 indicates equal opposing fluxes.

In the alongshore the suspended sediment flux by tidal asymmetry is small compared to the residual flux (figure 6.8 a&c). In the cross-shore, the suspended sediment flux generated by tidal asymmetry is larger during some periods than during other period (figure 6.8 b). The suspended sediment flux generated by tidal asymmetry is during those periods not always in the same direction as the residual flux. This means that tidal asymmetry does determine the transport direction at some moments in time. However, during periods when suspended sediment transport is large, the residual suspended sediment flux is dominant over the suspended sediment flux caused by tidal asymmetry (figure 6.7b and 6.8b). This means that the direction of the transport in the cross-shore is, like the direction of the transport in the alongshore, determined by the residual suspended sediment flux during most of the measurement period. Only in the cross-shore, this residual transport seems not to be only related to wind direction.

Periods with opposing cross-shore currents in the top and bottom of the water column where investigated in chapter 5. These periods could have an effect of the transport direction in the cross-shore. However, during periods where large cross-shore velocities differences over depth are measured, wind and wave activity is low (figure 6.9). During

periods with low wind and wave activity, the concentrations are also low and thus suspended sediment transport will also be low (figure 6.9). Periods with large cross-shore velocity differences over depth are not associated with periods of large suspended sediment transport.

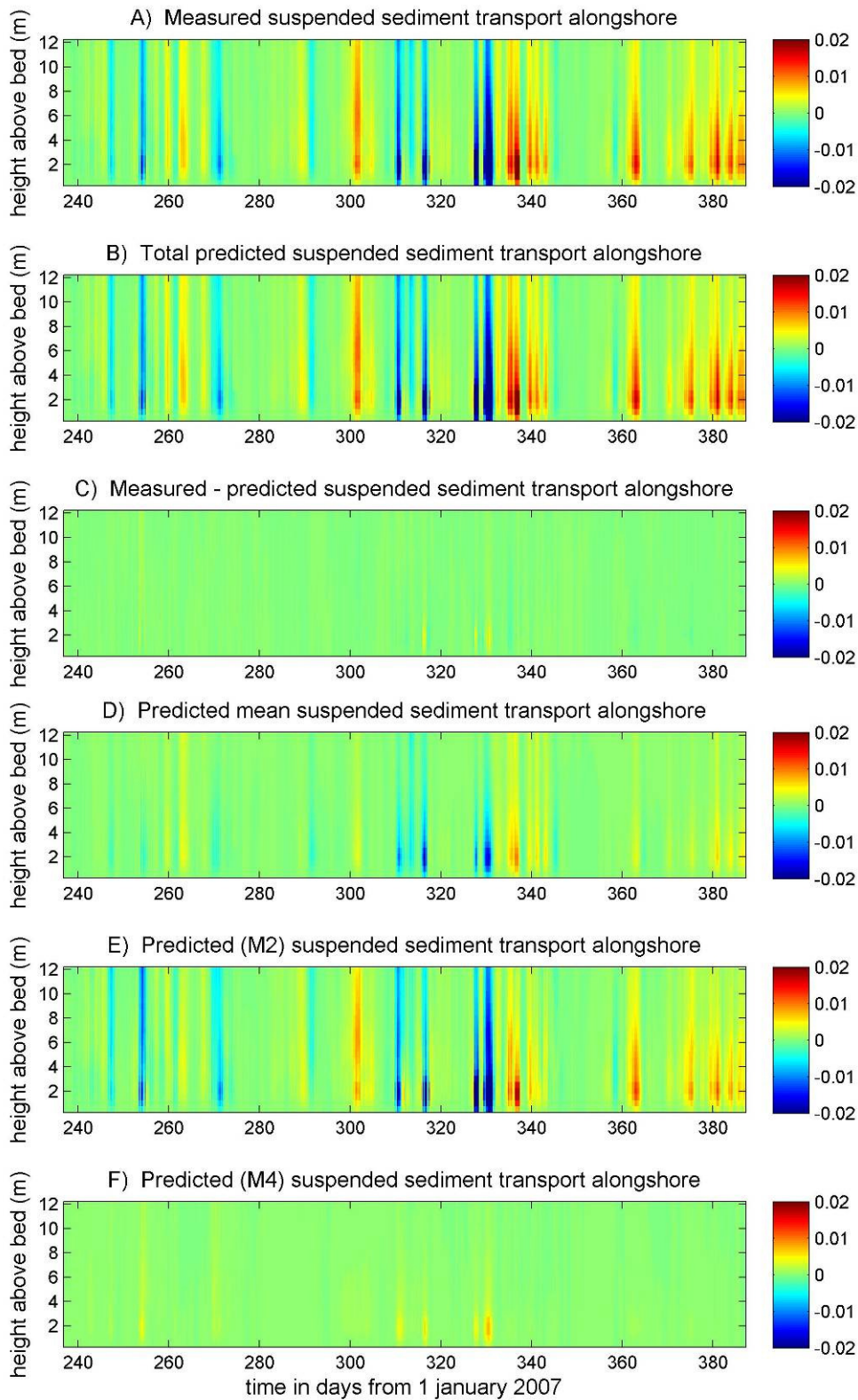


Figure 6.5: (a) Measured suspended sediment transport in the alongshore (positive to the north) during the whole measurement period, (b) predicted suspended sediment transport according to equation 6.2, (c) difference between measured and predicted transport, (d) the mean suspended sediment transport, (d&e) the suspended sediment transport by the M2 and M4 tidal cycle. All in $\text{kg}/(\text{m}^2\text{s})$.

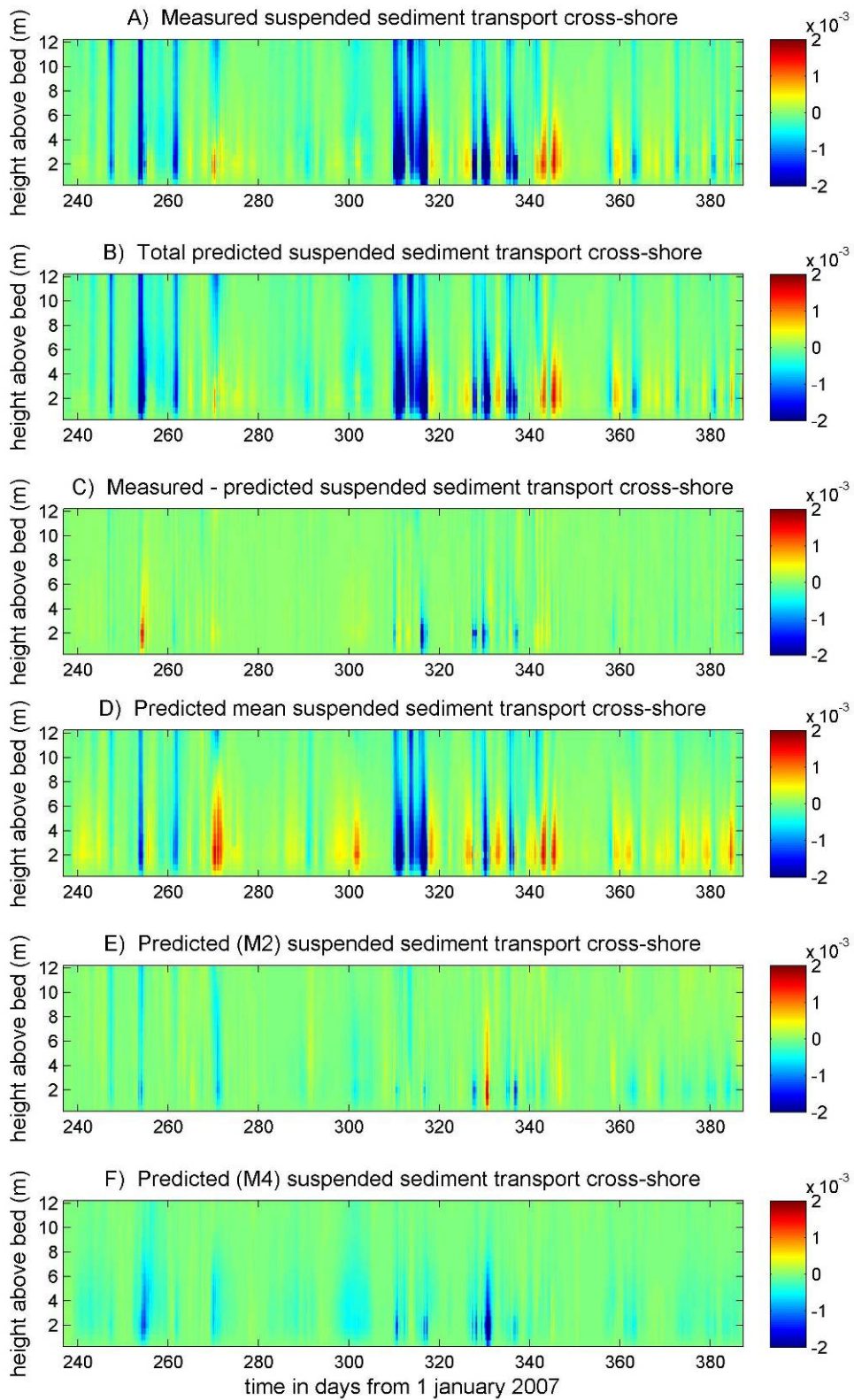


Figure 6.6: (a) Measured suspended sediment transport in the cross-shore (positive onshore) during the whole measurement period, (b) predicted suspended sediment transport according to equation 6.2, (c) difference between measured and predicted transport, (d) the mean suspended sediment transport, (d&e) the suspended sediment transport by the M2 and M4 tidal cycle. Note: The scale is ten times as small as in figure 6.5, the alongshore suspended sediment transport. All in $\text{kg}/(\text{m}^2\text{s})$.

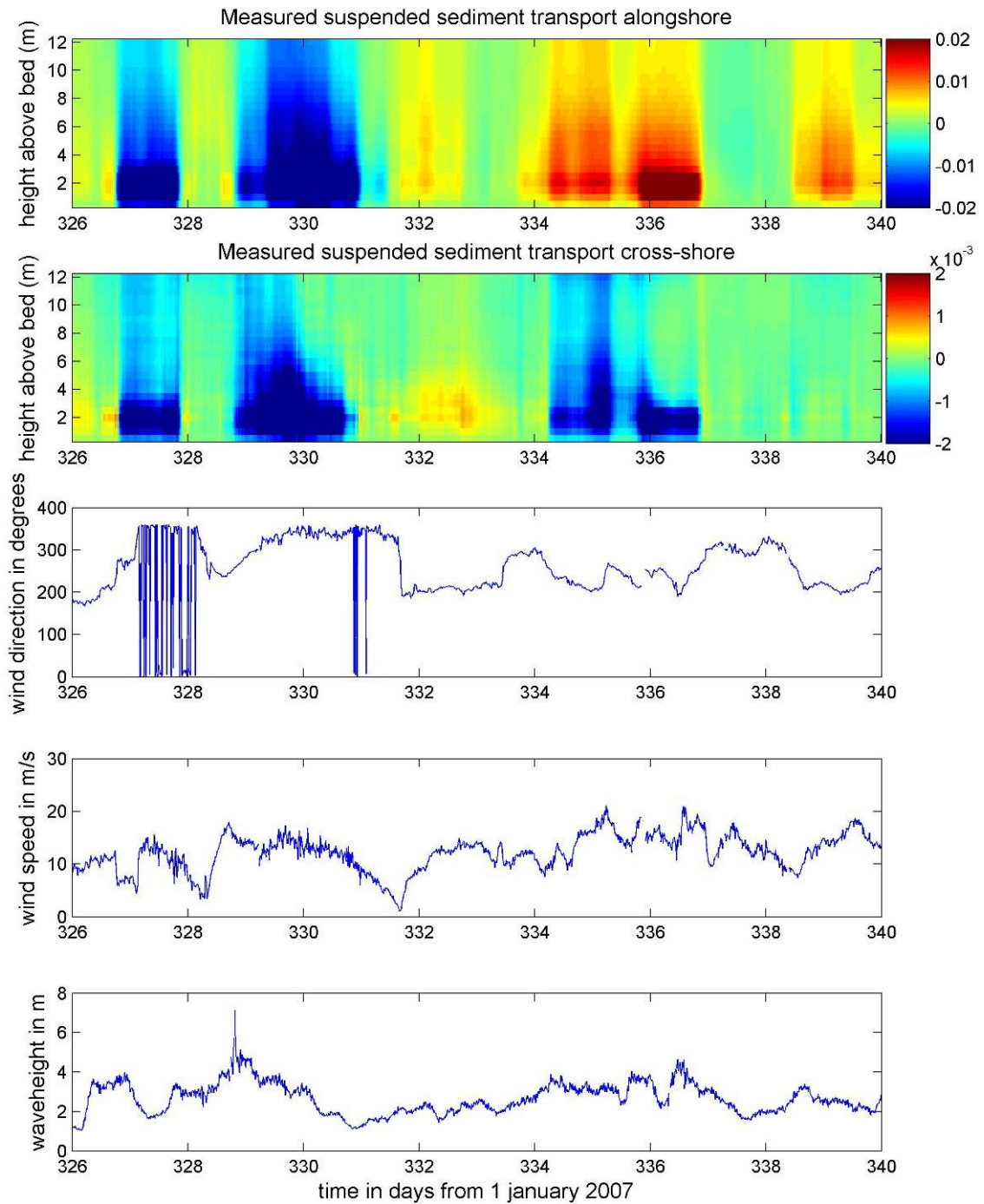


Figure 6.7: Suspended sediment transport in the alongshore and cross-shore (top) plotted together with the wind direction in degrees from the north, wind speed in m/s and wave height in m, for 14 days.

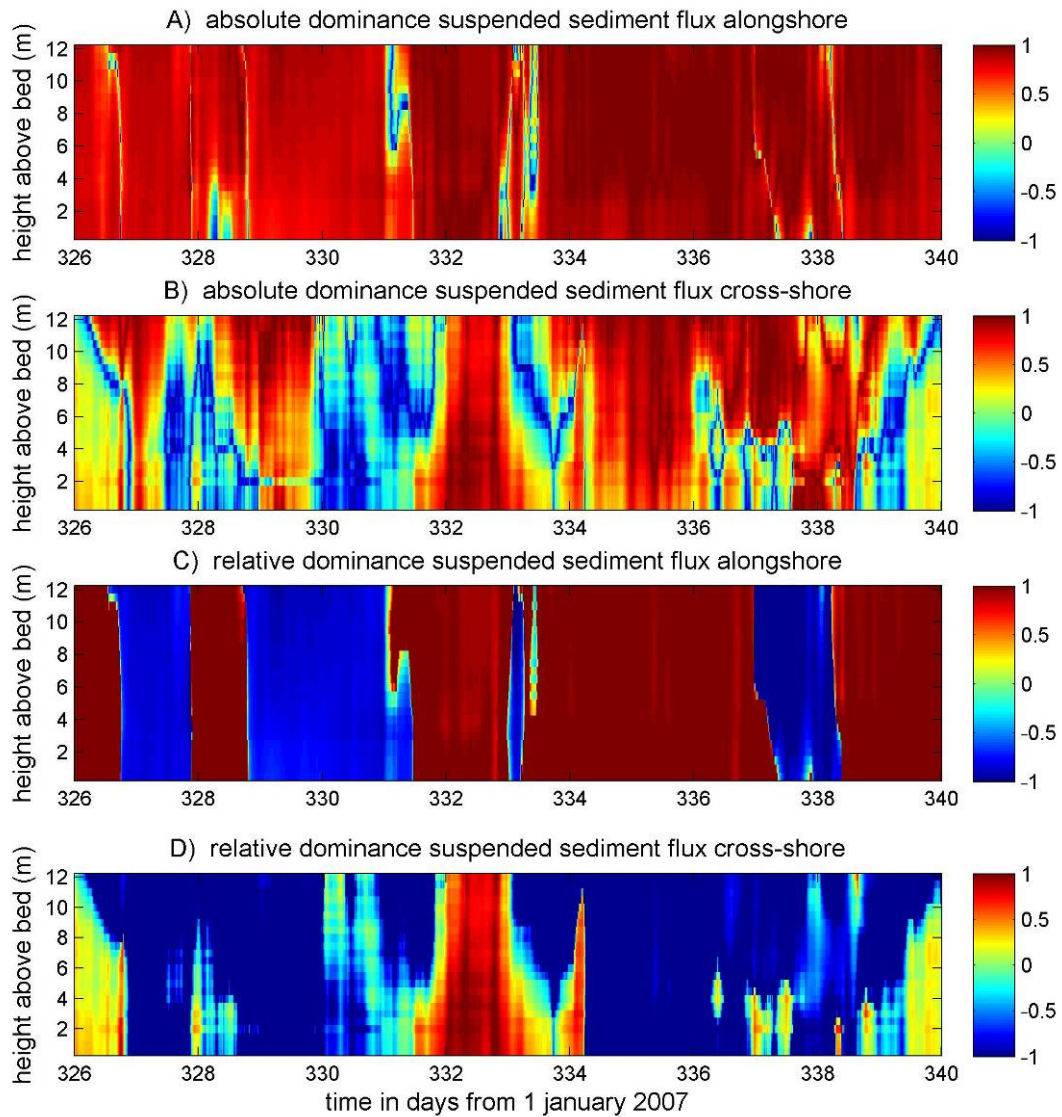


Figure 6.8: (A and B) The absolute dominance the transport by tidal asymmetry versus the residual transport of the suspended, value of 1 indicating a dominance of residual transport, value of -1 indicating dominance by tidal asymmetry. (C and D) Same as A and B, but than relative dominance, with a value of 1 indicating both residual as tidal asymmetry flux to the north, a value of -1 indicating both residual as tidal asymmetry flux to the south and a value of 0 indicating opposing directions.

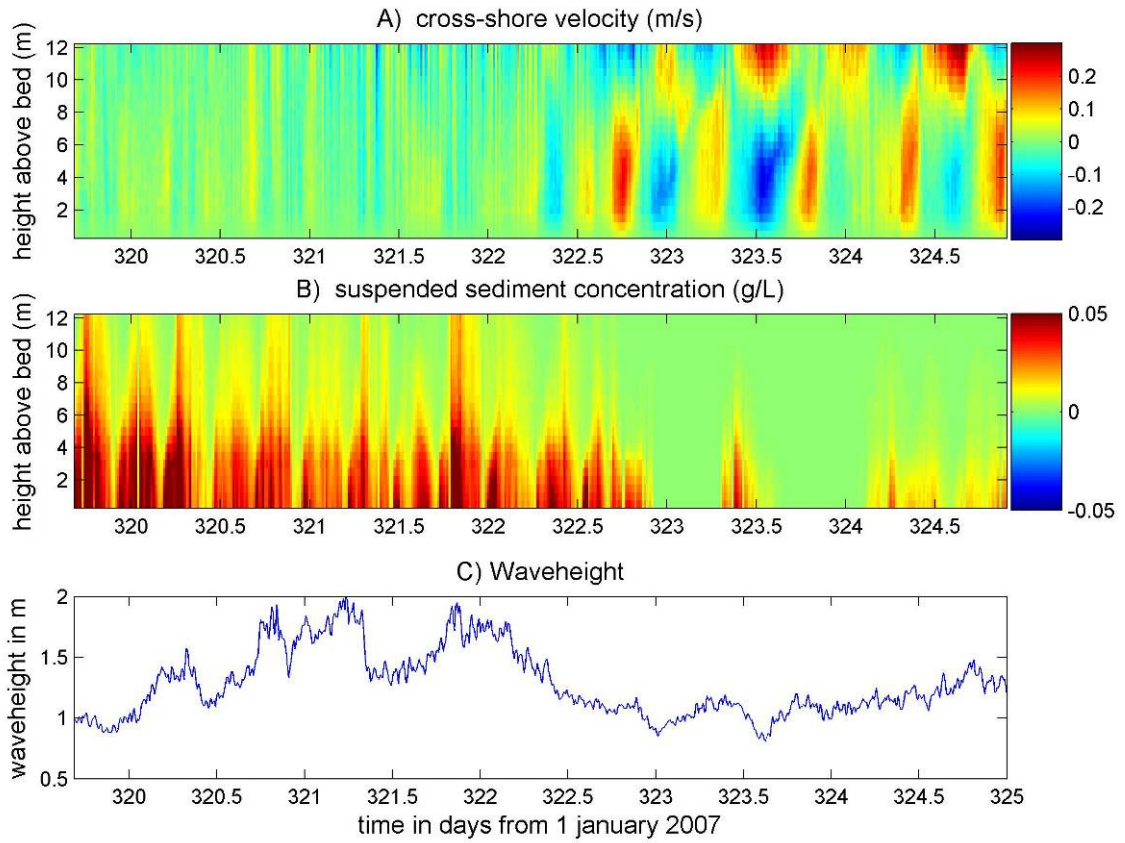


Figure 6.9: (A) Velocity in the cross-shore, (B) suspended sediment concentration and (C) wave height during 5 days with and without high cross-shore velocity differences.

7. Discussion

The aim of this paper was to extend the knowledge of suspended sediment transport along the Dutch coast. First the calibration of the ADCP will be discussed. Then the results on the hydrodynamics and suspended sediment concentration and transport will be discussed. In the end the influence of the Rhine on the suspended sediment transport along the Dutch coast is discussed.

7.1 ADCP calibration

The calibration of the ADCP was done with the assumption that particles in the water column are uniformly distributed under low current velocities and start to organise in clusters when the velocity is large. This was done to include the clustering of particles under high turbulent conditions, which return a stronger signal to the ADCP. The calibration parameter determines at which velocity the particles will be in the turbulent regime. Concentrations are determined with three different calibration parameters (figure 7.1).

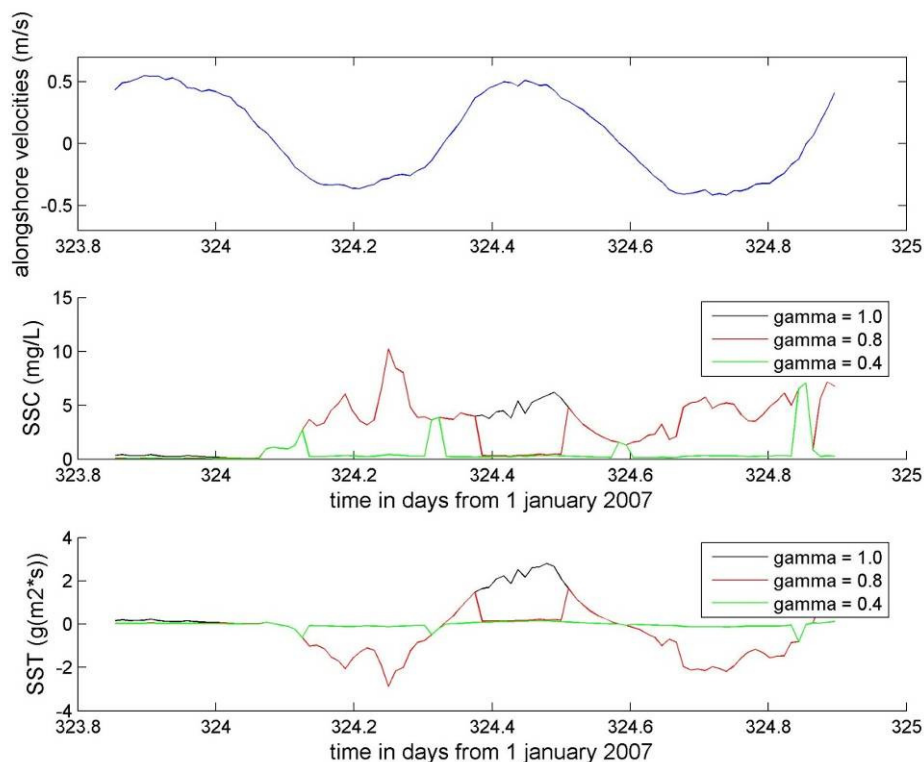


Figure 7.1: Alongshore velocities, depth averaged suspended sediment concentration and depth averaged suspended sediment transport (positive alongshore to the north) with $\gamma=0.4$, $\gamma=0.8$ and $\gamma=1.0$ for two M2 tidal cycles. The green line is on top of the red line, the red line is on top of the blue line.

When the calibration parameter is chosen at $\gamma=1.0$, then the particles are in the classical regime during day 324. When $\gamma=0.8$ the particles will be in the turbulent regime only when the absolute velocity is approximately 0.4 m/s. This is only during flood (figure 7.1). When $\gamma=0.4$, the particles will be in the turbulent regime when the absolute velocity is approximately 0.2 m/s (figure 7.1).

The calculation of the suspended sediment concentration of the turbulent regime results in much lower concentrations than the calculation of the classical regime. Therefore the calibration parameter determines for a large part the calculated concentrations. The calibration parameter also influences the suspended sediment transport magnitude and direction. With $\gamma=0.8$, the concentrations during flood are underestimated, while during ebb they are overestimated. This results in a net ebb directed transport during day 324 (figure 7.1). With $\gamma=1.0$ or $\gamma=0.4$, the concentrations over the whole day are respectively overestimated and underestimated, but this will have no influence on the calculated transport direction. Therefore during this study $\gamma=1.0$ was used to perform analysis on the suspended sediment concentration and transport.

The calibration parameter could also be determined with the calibration measurement. However there was only one 2.5 hour calibration measurement. To determine the calibration parameter correctly, there should have been more and longer calibration measurements. The characteristics of the suspended material in the water column will not be constant over time, so the transition from classical to turbulent regime will also not be constant over time. Therefore calibration measurements during several moments during the measurement period should have been executed in order to calibrate the ADCP for suspended sediment concentration.

The calibration measurement was done when tidal currents were low. The calibration measurements should also be over a full M2 tidal cycle, 12.5 hours, to perform measurements of the whole range of tidal amplitudes. Then the transition between classical and turbulent regime can be determined more precise.

Another reason why the calibration parameter could not be determined well is caused by the simplified formulas to determine the turbulent energy in the water column (eq. 5 and 6). Merckelbach and Ridderinkhof (2006) used these formulas for the Marsdiep tidal inlet. The water depth in the Marsdiep is more than two times as large as the water depth at the measurement location near IJmuiden. Winds and wave have more effect on the turbulent energy in the water column with shallower water depth. This probably has also effect on the transition from classical to turbulent regime at the measurement location.

7.2 Hydrodynamics

The flood directed current is larger than the ebb directed current. The flood current lasts shorter than the ebb directed current. This is caused by the interaction of the M2 tidal constituent and the M4, M6 and M8 tidal constituent. This results in tidal asymmetry, where the flood tidal amplitude is larger than the ebb tidal amplitude and the ebb period lasts longer than the flood period. In the cross-shore the average flow is onshore near the bottom and offshore at the top.

The currents in the alongshore are for a large part determined by the tidal motion. The currents in the cross-shore are less determined by tidal motion. This can be caused by either wind induced processes or buoyancy driven processes, which change the current pattern.

Wind direction influences the direction of the residual current in the alongshore direction. During periods with south-western and south-eastern winds the direction of the residual current is to the north. During periods with north-western and north-eastern winds the direction of the residual current is to the south. The transport direction has the same orientation in the top and bottom of the water column in alongshore direction.

The residual current direction in the cross-shore is not only dependent on wind direction. During both onshore and offshore winds, the direction of the cross-shore current is offshore at the top of the water column and onshore near the bottom. Not the wind, but another mechanism determines the direction of the residual current in the cross-shore.

The input of fresh water can result in density driven circulation which can cause the current difference in the cross-shore direction in the top and bottom of the water column. The relative fresh water which floats on top of the relative saline water will flow offshore. As a result, there will be an onshore current near the bottom of the water column. De Boer et al. (in press) observed a warm water mass moving offshore and upwelling of cold water near the Dutch coast. They concluded that this was an indication of stratification of the water column and a resulting density driven circulation.

The current structure is used as an indication of stratification as there were no temperature or salinity measurements over depth. The analysis of the tidal ellipses gives a measure for the stratification of the water column. There are strong tidal ellipse differences between top and bottom of the water column when there is also a strong difference in cross-shore current direction between top and bottom of the water column. There are periods with large ellipticity difference between top and bottom of the water column when wind stresses and tidal current amplitudes are small.

An exception is the period around day 350, when there is a period of high ellipticity, but the tidal currents are high and wind velocity is moderate. A flood wave of the river Rhine

could have caused a large input of fresh water into the Dutch coastal area and a buoyancy driven flow up to IJmuiden, although mixing in the water column was still high around day 350.

The measurement location is approximately 70 km to the north of the river mouth. A flood wave passing Lobith can have reached 58 km north of the river mouth with a depth averaged alongshore current of 4.2 m/s over the period between the fresh water entering the North Sea and maximum ellipticity differences. As buoyant water will be transported in the top of the water column and velocities will be higher in the top of the water column, it is plausible that this fresh water mass reached further north during the same period. The maximum amount of fresh water near the measurement location probably coincided with maximum differences in ellipticity between top and bottom of the water column.

The fresh water input in the North Sea influences the cross-shore current structure according to the indications of stratification. During periods with high ellipticity differences between top and bottom of the water column the cross-shore circulation is large. A cross-shore circulation cell is visible during periods with low mixing of the water column or when fresh water input is large.

7.3 *Suspended sediment*

The suspended sediment concentrations have a semi-diurnal tidal variation. Sediment will erode from the bottom and settle each tidal cycle. The concentrations are higher during flood than during ebb, due to a larger flood current than the ebb current.

The tidal mean suspended sediment concentrations relate to wave height. When wave height is large, stirring of bottom sediment is large and suspended sediment concentrations increase. When wave height is small, stirring of the water column is small and the suspended sediment will settle.

The suspended sediment transport direction in the alongshore is to a large extent determined by the residual current direction. Tidal asymmetry is not a dominant transport mechanism in the alongshore. So with northern wind the suspended sediment will be transported southward and with southern wind the suspended sediment will be transported to the north.

Suspended sediment transport in the cross-shore is relative small compared to the transport in the alongshore. Transport caused by tidal asymmetry is larger in the cross-shore than in the alongshore.

The suspended sediment transport in the cross-shore is not directly related to wind direction (figure 6.7). With northern winds, the transport direction is directed offshore. With south-western winds, the transport direction can be both onshore and offshore. The direction of the residual current is also not related to tidal asymmetry as this is a small component relative to the residual transport. The suspended sediment transport in the cross-shore could also be influenced by the periods with strong cross-shore circulation. Strong cross-shore circulation occurs when turbulence is low. When turbulence is low, the suspended sediment concentration will also be low. So transport during periods with strong cross-shore circulation is low. Cross-shore suspended sediment transport is thus mostly determined by wind and wave magnitude and direction and not by cross-shore circulation associated with fresh water input.

7.4 Influence of Rhine outflow on suspended sediment transport

There are indications of stratification near the measurement location. There is a cross-shore circulation when turbulence in the water column is low. This circulation can be a buoyancy driven circulation. There is also one event when there is a strong circulation while wave height is moderate and tidal current amplitudes are large. This could be caused by a large input of fresh water from the river Rhine. This means that the fresh water can also influence the current structure along the Dutch coast when there is mixing caused by tidal currents and waves.

The suspended sediment transport is determined by wind direction and magnitude. The suspended sediment is transported in the direction of the residual current. When suspended sediment concentration is large and the residual current is large, the transport will be large. This is during periods with large winds and waves, so when turbulence in the water column is large. During these periods there is no influence of fresh water on the residual current, so also no influence on the suspended sediment transport. Therefore the input of fresh water from the river Rhine into the North Sea seems not to have influence on the net suspended sediment transport.

However, if the water column can still become stratified when turbulence is high due to a large import of fresh water than the resulting cross-shore circulation does have influence on the transport of suspended sediment.

8. Conclusions

Will a change in outflow of fresh water into the North Sea result in a change in suspended sediment import into the Wadden Sea? To give an answer to this main question of this thesis first the results on the hydrodynamics and suspended sediment concentrations and transport will be given. Then an answer of the influence of the river Rhine on suspended sediment transport and the import of suspended sediment to the Wadden Sea is given.

8.1 Hydrodynamics

The alongshore depth averaged velocity is 2.1 cm/s to the north. In the alongshore the residual current is determined by wind direction. With southern winds the residual current is to the north. With northern winds, the current direction is to the south.

There is no depth averaged residual current in the cross-shore, but there is a mean offshore current near the top and a counteracting current near the bottom during the measurement period. These opposing currents are strong during periods with little turbulence in the water column, when wind velocity is small and tidal current amplitude is small. There is no cross-shore circulation. When turbulence is large, wind velocity is large and tidal current amplitude is large.

The cross-shore circulation seems to be related to stratification by fresh water input from the river Rhine. During one period around day 350 the cross-shore circulation was large, while turbulence induced by wind and tidal currents was also large. This could be related to a large input of fresh water by the river Rhine.

8.2 Suspended Sediment

The suspended sediment transport is a factor of tidal currents and the suspended sediment concentration. When the residual current is large and the concentrations are large, the suspended sediment transport will be large. Large residual currents and concentrations occur during periods when turbulence is large: with large wind velocities, with large wave height and when tidal current amplitudes are large.

The suspended sediment transport direction is related to wind direction, as the residual current is also related to wind direction. With northern winds, the suspended sediment transport will be to the south. With southern winds the suspended sediment transport will be to the north.

During periods with large suspended sediment transport, the turbulence in the water column is also large. There will be no cross-shore circulation when turbulence is large, so the residual transport in the cross-shore will almost not be influenced by the periods with cross-shore circulation. As it is assumed that the cross-shore circulation is a result of fresh water input in the North Sea, this input seems not to influence the cross-shore suspended sediment transport.

8.3 Influence of the Rhine on suspended sediment transport along the Dutch coast:

The input of fresh water into the North Sea does influence the hydrodynamics along the Dutch coast, but it does not strongly influence the suspended sediment transport. The alongshore suspended sediment transport is determined by the residual current which is determined by the wind velocity and direction. So also the alongshore suspended sediment transport seems not to be strongly influenced by the input of fresh water into the North Sea.

8.4 Influence of the Rhine on suspended sediment import to the Wadden Sea:

As the input of Rhine water does not seem to influence the suspended sediment along the Dutch coast, it also does not influence the input of suspended sediment into the Wadden Sea. A change in fresh water input into the North Sea, by changing the outflow of the river Rhine, will not influence the import of suspended sediment into the Wadden Sea.

9. Literature

9.1 Literature

- Asselman, N.E.M. (1999), *Suspended sediment dynamics in a large drainage basin: the River Rhine*, Hydrological Processes, vol. 13, p. 1437-1450
- Bagnold, R.A. (1966), *an approach to the sediment transport problem from general physics*, geological survey professional paper, vol. 422-I
- De Boer, G.J., et al. (2007), *SST observations of upwelling induced by tidal straining in the Rhine*, Continental Shelf Research, doi:10.1016/j.csr.2007.06.011
- De Ruijter, W.P.M., Van der Giessen, A., Groenendijk, F.C., (1992). Current and density structure in the Netherlands coastal zone. In: Prandle, D. (Ed.), Dynamics and Exchanges in Estuaries and the Coastal Zone. Am. Geophys. Union, Coastal Estuarine Sci., pp. 529-550.
- De Ruijter, W.P.M.; Visser, A.W. and Bos, W.G. (1997), *The Rhine outflow: A prototypical pulsed discharge plume in a high energy shallow sea*, Journal of Marine Systems, vol. 12, p. 263-276
- Elias, E.P.L., Cleveringa, J., Buijsman, M.C., Roelvink, J.A., Stive, M.J.F. (2006), *Field and model data analysis of sand transport patterns in Texel Tidal inlet (the Netherlands)*, Coastal Engineering, vol. 53, p. 505–529
- Flinchem, E.P. and Jay, D.A. (2000), *An Introduction to Wavelet Transform Tidal Analysis Methods*, Estuarine, Coastal and Shelf Science, 51, p. 177–200
- Fisher, N.R. and Simpson, J.H. (2002), M.J. Howarth, *Turbulent dissipation in the Rhine ROFI forced by tidal flow and wind stress*, Journal of Sea Research 48, p. 249–258
- Gerritsen, H., Vos, R.J., Van der Kaaij, T., Lane, A., Boon, J.G. (2000), *Suspended sediment modelling in a shelf sea: North Sea*, Coastal Engineering vol. 41 p. 317–352
- Gordon, R.L., *Acoustic Doppler Current Profiler, Principles of operation, a practical primer*, RD Instruments 1996
- Joordens, J.C.A.; Souza, A.J. and Visser, A. (2001), *The influence of tidal straining and wind on suspended matter and phytoplankton distribution in the Rhine outflow region*, Continental Shelf Research, Vol. 21, p. 301-325
- Lee, G.H., Dade, W.B., Friedrichs, C.T., Vincent, C.E. (2003), *Spectral estimates of bed shear stress using suspended-sediment concentrations in a wave-current boundary layer*, Journal of Geophysical Research, Vol. 108 (c7), p. 1-15

- Marchuk, G.I., Kagan, B.A. (1994), *Ocean tides, mathematical models and numerical experiments*, Pergamon Press
- Merckelbach, L.M. and Ridderinkhof, H. (2006), *Estimating suspended sediment concentration using backscatterance from an acoustic Doppler profiling current meter at a site with strong tidal currents*, *Ocean Dynamics*, vol. 56 p. 153-168
- Middelkoop, H. (red), (1998), *Twee rivieren: Rijn en Maas in Nederland*, RIZA rapport 98.041, 121p., Arnhem: RIZA
- Pawlowicz, R., Beardsley, B. Lentz, S. (2002), *Classical tidal harmonic analysis including error estimates in MATLAB using T TIDE*, *Computers & Geosciences* 28 p929–937
- Pugh, David T. (1987), *Tides, surges and mean sea-level*. John Wiley and Sons, 472 p.
- Simpson, J.H. (1997), *Physical processes in the ROFI regime*, *Journal of Marine Systems*, vol. 12, p. 3-15
- Souza, A. J. and Simpson, J. H. (1995), *The modification of tidal ellipses by stratification in the Rhine ROFI*, *Continental Shelf Research*, vol. 16 (8), p. 997-1007
- Terwindt, J.H.J. (1967), *Mud transport in the Dutch delta area and along the adjacent coastline*, *Netherlands Journal of Sea Research*, vol. 3, p. 505-531
- Terwindt, J.H.J. (1977), *Mud in the Dutch delta area*, *Geologie en Mijnbouw*, vol. 56 p203-210
- Torrence and Compo (1998), *a practical guide to wavelet analysis*, *Bulletin of the American Meteorological Society*, Vol. 79 (1), p. 61-78
- Van Alphen, J.S.L.J., De Ruijter, W.P.M. and Borst, J.C. (1988), *Outflow and three-dimensional spreading of Rhine River water in the Netherlands coastal zone*, *Physical Processes in Estuaries*, Springer-Verlag, p. 70-92
- Van Alphen, J.S.L.J. (1990), *A mud balance for Belgian-Dutch coastal waters between 1969 and 1986*, *Netherlands Journal of Sea Research*, vol. 25, p. 19-30
- Van de Kreeke, J., Day, C.M., Mulder, H.P.J. (1997), *Tidal variations in suspended sediment concentration in the Ems estuary: origin and resulting sediment flux*, *Journal of Sea Research*, Vol. 38, p. 1-16
- Van der Giessen, A.; De Ruijter, W.M.P. and Borst, J.C. (1990), *three dimensional current structure in the Dutch coastal zone*, *Netherlands Journal of Sea Research*, vol. 25, p. 45-55
- Van Haren, H. (2001), *Estimates of sea level, waves and winds from a bottom-mounted ADCP in a shelf sea*, *Journal of Sea research*, vol. 45, p. 1-14
- Van Straaten I.M.J.U. and Kuenen, Ph.H. (1957), *accumulation of fine grained sediments in the Dutch Wadden Sea*, *Geologie en Mijnbouw*, vol. 19, p. 329-354
- Visser, M.; De Ruijter, W.P.M. and Postma, L. (1991), *The distribution of suspended matter in the Dutch coastal zone*, *Netherlands Journal of Sea Research*, vol. 27 (2), p. 127-143

Visser, M.; De Ruijter, W.P.M. and Postma, L. (1991), *The distribution of suspended matter in the Dutch coastal zone*, *Netherlands Journal of Sea Research*, vol. 27 (2), p. 127-143

9.2 Websites

Rijkswaterstaat hydrological data: www.waterbase.nl